Struct Multidisc Optim (2007) 34:91–110
DOI 10.1007/s00158-007-0101-y

RESEARCH PAPER

Topological design of freely vibrating continuum structures for maximum values of simple and multiple eigenfrequencies and frequency gaps

Jianbin Du · Niels Olhoff

Received: 30 June 2005 / Accepted: 1 December 2006 / Published online: 3 May 2007

Abstract A frequent goal of the design of vibrating structures is to avoid resonance of the structure in a given interval for external excitation frequencies. This can be achieved by, e.g., maximizing the fundamental eigenfrequency, an eigenfrequency of higher order, or the gap between two consecutive eigenfrequencies of given order. This problem is often complicated by the fact that the eigenfrequencies in question may be multiple, and this is particularly the case in topology optimization. In the present paper, different approaches are considered and discussed for topology optimization involving simple and multiple eigenfrequencies of linearly elastic structures without damping. The mathematical formulations of these topology optimization problems and several illustrative results are presented.

Keywords Eigenfrequency design · Multiple eigenvalues · Topology optimization · Bound formulation

1 Introduction

Problems of passive design against vibrations and noise were already undertaken some decades ago in the papers (Olhoff 1976, 1977) in the form of shape optimization of transversely vibrating beams with respect to fundamental and higher order eigenfrequencies. By optimizing with respect to the fundamental eigenfrequency, minimum cost designs against vibration resonance were obtained subject to all external excitation frequencies within the large range from zero and up to the particular optimum fundamental eigenfrequency. Optimization with respect to a higher order eigenfrequency was found to produce a considerable gap between the subject eigenfrequency and the adjacent lower eigenfrequency, and this approach offered even more competitive designs for avoidance of resonance in problems where external exitation frequencies are confined within a large interval with finite lower and upper limits. In the subsequent papers of Olhoff and Parbery (1984) and Bendsøe and Olhoff (1985), the design objective was directly formulated as maximization of the separation (gap) between two consecutive eigenfrequencies of the beam.

Topology optimization with respect to eigenfrequencies of structural vibration was first considered by Diaz and Kikuchi (1992), who dealt with single frequency design of plane disks. Subsequently, Ma et al. (1994, 1995), Diaz et al. (1994), and Kosaka and Swan (1999) presented different formulations for simultaneous maximization of several frequencies of free vibration of disk and plate structures, defining the objective function as a scalar weighted function of the eigenfrequencies. In contrast to this, the more recent papers of Krog and Olhoff (1999) and Jensen and Pedersen (2006) apply a variable bound formulation that facilitates proper treatment of multiple eigenfrequencies that very often result from the optimization. The paper of Krog and Olhoff (1999) treats optimization of fundamental and higher order eigenfrequencies of disk and plate structures, and the paper of Jensen and Pedersen (2006) deals with maximization of the separation of adjacent eigenfrequencies for bimaterial plates. The paper of Pedersen (2000) deals with maximum fundamental eigenfrequency design of plates and includes a technique to avoid spurious localized modes.

J. Du · N. Olhoff (✉)
Department of Mechanical Engineering, Aalborg University,
9220, Aalborg East, Denmark
e-mail: no@ime.aau.dk

J. Du
e-mail: jd@ime.aau.dk

It should be noted that the separation of adjacent eigenfrequencies as considered by Jensen and Pedersen (2006) and in this paper is closely related to the existence of so-called phononic (or acoustic) band gaps, i.e., gaps in the wave band structure for periodic materials, implying that elastic waves cannot propagate in certain frequency ranges. Sigmund (2001) has applied topology optimization to maximize phononic band gaps in periodic materials, and Sigmund and Jensen (2003) have performed minimization of the response of band gap structures (wave damping).

Methods for optimization of simple eigenvalues/eigenfrequencies in shape and sizing design problems are well established and can be implemented directly in topology optimization. However, particularly in topology optimization, it is often found that, although an eigenfrequency is simple during the initial stage of the iterative design procedure, later it may become multiple because of the coincidence of this eigenfrequency with one (or more) of its adjacent eigenfrequencies. To capture this behavior, it is necessary to apply a more general solution procedure that allows for the multiplicity of the eigenfrequency, because such an eigenfrequency does not possess usual differentiability properties.

In the present paper, the topology optimization problems involving simple and multiple eigenfrequencies is formulated by a bound formulation (Bendsøe et al. 1983; Taylor and Bendsøe 1984; Olhoff 1989), and the calculation of design sensitivities of multiple eigenfrequencies is based on results published in Seyranian et al. (1994). The problems can then be solved efficiently by mathematical programming (see, e.g., Overton 1988; Olhoff 1989) or the method of moving asymptotes (MMA) (Svanberg 1987). Moreover, the procedure of treating the multiple eigenvalues can be greatly simplified by using the increments of the design variables as unknowns (Krog and Olhoff 1999).

The material of the paper is organized as follows. Section 2 gives a brief account of the SIMP (solid isotropic microstructure with penalty) material models used in this paper. An extended form of the SIMP model for handling of bimaterial topology design is also included. In Section 3, structural topology optimization subject to prescribed volume of the material is first considered for problems of maximizing the fundamental or a higher order eigenfrequency, and then problems of maximizing the distance (gap) between two consecutive eigenfrequencies are considered. Section 3 also presents topological design sensitivity results for simple and multiple eigenfrequencies, and the computational procedure for solution of the optimization problems is discussed. Section 4 presents several examples of single material optimum topology designs of beam-like 2D structures and also includes an example that shows the superiority of the method proposed in the present paper relative to early approaches of topological design with respect to eigenfrequencies. Section 5 presents a number of both single- and bimaterial optimum topology designs of plate-like 3D structures. Finally, Section 6 concludes the paper.

2 Material interpolation for topology optimization of vibrating structures

Topology optimization is basically a problem of discrete optimization, but this difficulty is avoided by introducing relationships between stiffness components and the volumetric density of material ρ, which is a continuous variable defined between limits 0 (corresponding to void) and 1 (corresponding to solid elastic material) over the admissible design domain. The aim of the optimization process is to determine the optimum zero (void)–one (solid) distribution of a prescribed amount of the given material over the admissible design domain. To achieve this goal, many different material models have been developed (see, e.g., Eschenauer and Olhoff 2001; Bendsøe and Sigmund 2003; Bendsøe et al. 2006), among which the SIMP model (see, e.g., Bendsøe 1989; Rozvany and Zhou 1991; Rozvany et al. 1992; Bendsøe and Sigmund 1999) is a simple and effective one, which is widely used in optimum topology design. With a view to prevent checkerboard formation and dependency of the optimum solutions on finite element refinement, the mesh-independent filter developed by Sigmund (1997), see also Sigmund and Petersson (1998), has been applied to the sensitivities of the objective functions in the computational models in the paper.

2.1 SIMP model for topology optimization of single-material structures

According to the SIMP model, the finite element elasticity matrix $\mathbf{E}_e$ is expressed in terms of the element volumetric material density ρ_e, $0 \le \rho_e \le 1$, in a power p, $p \ge 1$, as

$$\mathbf{E}_e(\rho_e) = \rho_e^p \mathbf{E}_e^*, \tag{1}$$

where $\mathbf{E}_e^*$ is the elasticity matrix of a corresponding element with the fully solid elastic material the structure is to be made of. The power p in (1), which is termed the penalization power, is introduced with a view to yield distinctive "0–1" designs, and is normally assigned values increasing from 1 to 3 during the optimization process. Such values of p have the desired effect of penalizing intermediate densities $0<\rho_e<1$, as the element material volume is proportional to ρ_e, whereas the interpolation (1) implies that the element stiffness is less than proportional. Note also that the interpolation (1) satisfies $\mathbf{E}_e(0)=0$ and $\mathbf{E}_e(1)=\mathbf{E}_e^*$, implying that if a final design has density 0 and 1 in all elements, this is a design for which the structural response has been evaluated with a correct physical model.

By analogy with (1), for a vibrating structure, the finite element mass matrix may be expressed as

$$\mathbf{M}_e(\rho_e) = \rho_e^q \mathbf{M}_e^*, \tag{2}$$

where $\mathbf{M}_e^*$ represents the element mass matrix corresponding to fully solid material, and the power $q \geq 1$. Apart from exceptions briefly discussed in the following section, normally, $q=1$ is chosen.

The global stiffness matrix $\mathbf{K}$ and mass matrix $\mathbf{M}$ for the finite element-based structural response analyses behind the optimization can now be calculated by

$$\mathbf{K} = \sum_{e=1}^{N_E} \rho_e^p \mathbf{K}_e^*, \quad \mathbf{M} = \sum_{e=1}^{N_E} \rho_e^q \mathbf{M}_e^*. \tag{3}$$

In this equation, K_e^* is the stiffness matrix of a finite element with the fully solid material for the structure, and N_E denotes the total number of finite elements in the admissible design domain.

2.2 Localized eigenmodes

With values assigned to p and q as stated above, application of the SIMP model for problems of topology optimization with respect to eigenfrequencies may lead to the occurrence of spurious, localized eigenmodes associated with very low values of corresponding eigenfrequencies. The localized eigenmodes may occur in subregions of the design domain with low values of the material density (e.g., $\rho_e \leq 0.1$), where the ratio between the stiffness (with, say, $p=3$ in the interpolation formula) and the mass (with $q=1$) is very small. To eliminate these spurious eigenmodes, we may use the method of Pedersen (2000) of linearizing the element stiffness or the approach of Tcherniak (2002) of setting the element mass to 0 in subregions with low material density. Thus, following Tcherniak (2002) with a slight modification to avoid numerical singularity, the interpolation formula (2) for the finite element mass matrix was modified as

$$\mathbf{M}_e(\rho_e) = \begin{cases} \rho_e \mathbf{M}_e^*, & \rho_e > 0.1 \\ \rho_e^r \mathbf{M}_e^*, & \rho_e \leq 0.1 \end{cases}. \tag{4}$$

In this equation, the mass is set very low via a high value of the penalization power r in subregions with low material density. Thus, r is chosen to be about $r=6$, i.e., much larger than the penalization power p for the stiffness, which is kept unchanged at a value about $p=3$.

It is noted that (4) is discontinuous at the low value $\rho_e=0.1$ of the material density. Numerically, this is not a serious problem, as the discontinuity only occurs at a single point. However, we can always improve (4) by generating a continuous interpolation model for the mass with respect to any value of the material density between 0 and 1. For example, to achieve C^0 continuity of the interpolation model, we may introduce the following revised form of (4),

$$\mathbf{M}_e(\rho_e) = \begin{cases} \rho_e \mathbf{M}_e^*, & \rho_e > 0.1 \\ c_0 \rho_e^6 \mathbf{M}_e^*, & \rho_e \leq 0.1 \end{cases}, \tag{4a}$$

where the coefficient $c_0=10^5$ enforces the C^0 continuity at the value $\rho_e=0.1$ of the material density. If we wish to impose C^1 continuity on the interpolation model, we may replace (4) by the model

$$\mathbf{M}_e(\rho_e) = \begin{cases} \rho_e \mathbf{M}_e^*, & \rho_e > 0.1 \\ (c_1 \rho_e^6 + c_2 \rho_e^7) \mathbf{M}_e^*, & \rho_e \leq 0.1 \end{cases}, \tag{4b}$$

where the two coefficients $c_1=6\times10^5$ and $c_2=-5\times10^6$ ensure the C^1 continuity of the interpolation model. In several of the examples presented later in this paper, for comparison, we have applied each of the three different interpolation models, i.e., (4), (4a), and (4b) in the numerical solution scheme and only found negligible differences in the final results. The reason is that the region with lower density in all the three models has a very small contribution to the first several eigenfrequencies of the structure. Furthermore, all intermediate values of the material density will approach 0 or 1 during the design process, which implies that the changes of the interpolation model in regions with lower density as shown in (4a) or (4b) must have very limited influence on the final 0–1 design.

2.3 SIMP model for topology optimization of bimaterial structures

The SIMP model for topology optimization of structures made of two different solid elastic materials can be easily obtained by an extension of the SIMP model for single-material design. Following Bendsøe and Sigmund (1999), the finite element elasticity matrix for the bimaterial problem can be expressed as

$$\mathbf{E}_e(\rho_e) = \rho_e^p \mathbf{E}_e^{*1} + \left(1 - \rho_e^p\right) \mathbf{E}_e^{*2}, \tag{5}$$

where $\mathbf{E}_e^{*1}$ and $\mathbf{E}_e^{*2}$ denote the element elasticity matrices corresponding to the two given solid, elastic materials *1 and *2. In this equation, material *1 is assumed to be the stiffer one. The penalization power p in (5) was assigned the value 3 in this paper, which resulted in distinctive optimum topology designs in the examples of bimaterial design considered. It follows from (5) that for a given element, $\rho_e=1$ implies that the element fully consists of the solid material *1, whereas $\rho_e=0$ means that the element fully consists of the solid material *2.

The element mass matrix of the bimaterial model may be stated as the simple linear interpolation

$$\mathbf{M}_e(\rho_e) = \rho_e \mathbf{M}_e^{*1} + (1 - \rho_e) \mathbf{M}_e^{*2}, \tag{6}$$

where $\mathbf{M}_e^{*1}$ and $\mathbf{M}_e^{*2}$ are the element mass matrices corresponding to the two different, given solid elastic materials *1 and *2.

The SIMP model formulated by (1) and (2) (or (5) and (6)) may be regarded as an interpolation scheme for the structural stiffness and mass with respect to material volume density. Recently, a generalized material model based on a polynomial interpolation was proposed by Jensen and Pedersen (2006), and it was shown how proper polynomials corresponding to different design objectives can be easily obtained.

When bimaterial design is treated via the problem formulations in Sections 3 and 4, then V^* denotes the total volume $\sum_{e=1}^{N_E} \rho_e V_e$ of the stiffer material *1 available for the structure, whereas the total volume of material *2 is given by $V_0 - V^*$, where V_0 is the volume of the admissible design domain. In the figures in Section 4 presenting optimum topologies of bimaterial structures, material *1 is shown in black and material *2 in gray.

3 Formulations for eigenfrequency optimization problems

3.1 Maximization of the fundamental eigenfrequency

Problems of topology design for maximization of fundamental eigenfrequencies of vibrating elastic structures have, e.g., been considered in the papers (Diaz and Kikuchi 1992; Ma et al. 1994, 1995; Diaz et al. 1994; Kosaka and Swan 1999; Krog and Olhoff 1999; Pedersen 2000). Assuming that damping can be neglected, such a design problem can be formulated as a max–min problem as follows:

$$\max_{\rho_1,\cdots,\rho_{N_E}} \left\{ \min_{j=1,\cdots J} \left\{ \omega_j^2 \right\} \right\} \tag{7a}$$

subject to:

$$\mathbf{K}\phi_j = \omega_j^2 \mathbf{M}\phi_j, \quad j = 1,\cdots,J, \tag{7b}$$

$$\phi_j^{\mathrm{T}} \mathbf{M} \phi_k = \delta_{jk}, \quad j \geq k, \quad k,j = 1,\cdots,J, \tag{7c}$$

$$\sum_{e=1}^{N_E} \rho_e V_e - V^* \leq 0, \quad V^* = \alpha V_0, \tag{7d}$$

$$0 < \underline{\rho} \leq \rho_e \leq 1, \quad e = 1,\cdots,N_E. \tag{7e}$$

In these equations, ω_j is the jth eigenfrequency and ϕ_j the corresponding eigenvector, and $\mathbf{K}$ and $\mathbf{M}$ are the symmetric and positive definite stiffness and mass matrices of the finite element-based, generalized structural eigenvalue problem in the constraint (7b). The J candidate eigenfrequencies considered will all be real and can be numbered such that

$$0 < \omega_1 \leq \omega_2 \leq \cdots \leq \omega_J, \tag{8}$$

and it will be assumed that the corresponding eigenvectors are $\mathbf{M}$ orthonormalized, cf. (7c) where δ_{jk} is Kronecker's delta.

In problem (7a–e), the symbol N_E denotes the total number of finite elements in the admissible design domain. The design variables ρ_e, e=1,...,N_E represent the volumetric material densities of the finite elements, and (7e) specifies lower and upper limits $\underline{\rho}$ and 1 for ρ_e. To avoid singularity of the stiffness matrix, $\underline{\rho}$ is not 0 but taken to be a small positive value like $\underline{\rho}=10^{-3}$. In (7d), the symbol α defines the volume fraction V^*/V_0, where V_0 is the volume of the admissible design domain, and V^* is the given available volume of solid material and of solid material *1, respectively, for a single-material and a bimaterial design problem, cf. Sections 2.1 and 2.3.

3.2 Sensitivity analysis of a unimodal eigenfrequency

If the jth eigenfrequency ω_j is unimodal (also called simple or distinct), i.e., $\omega_{j-1} < \omega_j < \omega_{j+1}$, then the corresponding eigenvector ϕ_j will be unique (up to a sign) and differentiable with respect to the design variables ρ_e, e=1,...,N_E. To determine the sensitivity $(\lambda_j)'_{\rho_e}$ of the eigenvalue $\lambda_j = \omega_j^2$ with respect to a particular design variable ρ_e, we differentiate the vibration (7b) with respect to ρ_e, and get

$$\begin{aligned} &(\mathbf{K} - \lambda_j \mathbf{M})(\phi_j)'_{\rho_e} + \left(\mathbf{K}'_{\rho_e} - \lambda_j \mathbf{M}'_{\rho_e} - (\lambda_j)'_{\rho_e}\mathbf{M}\right)\phi_j = 0, \\ &e = 1,\cdots,N_E, \end{aligned} \tag{9}$$

where $()'_{\rho_e} = \partial()/\partial\rho_e$. Premultiplying (9) by ϕ_j^{T} and using the vibration equation (7b) and the normalization of ϕ_j included in (7c) then gives (see also Wittrick 1962; Lancaster 1964; Haftka et al. 1990)

$$(\lambda_j)'_{\rho_e} = \phi_j^T \left(\mathbf{K}'_{\rho_e} - \lambda_j \mathbf{M}'_{\rho_e}\right)\phi_j \quad e = 1,\cdots,N_E. \tag{10}$$

The derivatives of the matrices $\mathbf{K}$ and $\mathbf{M}$ can be calculated explicitly from the material models in Section 2. Considering, e.g., the single-material model in (3), the sensitivity of the eigenvalue $\lambda_j = \omega_j^2$ with respect to the design variable ρ_e becomes

$$\begin{aligned} &(\lambda_j)'_{\rho_e} = \phi_j^T \left(p\rho_e^{(p-1)}\mathbf{K}_e^* - \lambda_j q \rho_e^{(q-1)}\mathbf{M}_e^*\right)\phi_j, \\ &e = 1,\cdots,N_E. \end{aligned} \tag{11}$$

The optimality condition for the maximization of a unimodal eigenvalue $\lambda_j = \omega_j^2$ of given order j, j=1, 2, ...,

now follows from (10) (or (11)) and usage of the Lagrange multiplier method, and takes the form

$$\left(\lambda_j\right)'_{\rho_e} - \gamma_0 V_e = 0, \quad e = 1, \cdots, N_E \tag{12}$$

where γ_0 (≥ 0) is the Lagrange multiplier corresponding to the material volume constraint and the side constraints for ρ_e have been ignored. With this sensitivity result and optimality condition, the design problem (7a–e) may be solved for a unimodal optimum eigenfrequency by using an OC (Optimality Criterion) based method, e.g., the fixed point method (see Cheng and Olhoff 1982), or a mathematical programming method, e.g., MMA (Svanberg 1987).

We may also wish to apply a gradient based method of solution. It is then essential that the jth eigenvalue $\lambda_j = \omega_j^2$ is simple and differentiable, and thereby admits linearization with respect to the design variables ρ_e, e=1, ..., N_E. Hence, if all the design variables are changed simultaneously, the linear increment $\Delta\lambda_j$ of $\lambda_j = \omega_j^2$ is given by the scalar product

$$\Delta\lambda_j = \nabla\lambda_j^T \Delta\rho \tag{13}$$

where $\Delta\rho = \left\{\Delta\rho_1, \cdots, \Delta\rho_{N_E}\right\}^T$ is the vector of changes of the design variables ρ_e, e=1, ..., N_E, and

$$\nabla\lambda_j = \left\{\phi_j^T\left(\mathbf{K}'_{\rho_1} - \lambda_j \mathbf{M}'_{\rho_1}\right)\phi_j, \cdots\cdots, \phi_j^T\left(\mathbf{K}'_{\rho_{N_E}} - \lambda_j \mathbf{M}'_{\rho_{N_E}}\right)\phi_j\right\}^T \tag{14}$$

is the vector of sensitivities (or gradients) of the eigenvalue λ_j with respect to the design variables ρ_e, e=1, ..., N_E.

3.3 Bound formulations for maximization of the nth eigenfrequency or the distance between two consecutive eigenfrequencies

In this section, we first consider the more general problem of maximizing the nth eigenfrequency ω_n of given order of a vibrating structure, i.e., the fundamental eigenfrequency (n=1) or a higher order eigenfrequency (n>1). Employing a bound formulation (Bendsøe et al. 1983; Taylor and Bendsøe 1984; Olhoff 1989) involving a scalar variable β which plays both the role of an objective function to be maximized and at the same time a variable lower bound for the nth and higher order eigenfrequencies (counted with possible multiplicity), the above problem can be formulated as

$$\max_{\beta,\rho_1,\cdots,\rho_{N_E}} \{\beta\} \tag{15a}$$

subject to:

$$\beta - \omega_j^2 \leq 0, \quad j = n, n+1, \cdots, J \tag{15b}$$

$$\textit{Constraints}: \ 7(b-e) \tag{15c}$$

In these equations, as well as in (16a, 16b, 16c, 16d) below, J is assumed to be larger than the highest order of an eigenfrequency to be considered a candidate to exchange its order with the nth eigenfrequency or to coalesce with this eigenfrequency during the design process.

The problem of maximizing the distance (gap) between two consecutive eigenfrequencies of given orders n and $n-1$ (where n>1) may be written in the following extended bound formulation, where two bound parameters are used (see also Bendsøe and Olhoff 1985; Jensen and Pedersen 2006):

$$\max_{\beta_1,\beta_2,\rho_1,\cdots,\rho_{N_E}} \{\beta_2 - \beta_1\} \tag{16a}$$

subject to:

$$\beta_2 - \omega_j^2 \leq 0, \quad j = n, n+1, \cdots, J \tag{16b}$$

$$\omega_j^2 - \beta_1 \leq 0, \quad j = 1, \cdots, n-1, \tag{16c}$$

$$\text{Constraints}: \ 7(b-e). \tag{16d}$$

Note that if in (16a–d), we remove the bound variable β_1 and the corresponding set of constraints (16c) from the formulation, then the eigenfrequency gap maximization problem (16a–d) reduces to the nth eigenfrequency maximization problem (15a–c) and, in particular, for n=1, to the problem of maximizing the fundamental eigenfrequency in (7a–e).

In problem (15a–c), the eigenfrequency ω_n and in problem (16a–d), both the eigenfrequencies ω_n and ω_{n-1} of the optimum solution may very well be multiple, and the bound formulations in (15a–c) and (16a–d) are tailored to facilitate handling of such difficulties.

It is also worth noting that the introduction of the scalar bound variables β in (15a–c) and β_1 and β_2 in (16a–d) implies that even if multiple eigenfrequencies are present, the optimization problems (15a–c) and (16a–d) are both *differentiable* if they are considered as problems in *all* variables, i.e., the bound parameter(s) β (or β_1, β_2), the design variables ρ_e, e=1, $\cdots$, N_E, as well as the eigenfrequencies ω_j and eigenvectors ϕ_j, j=1, $\cdots$, J (implying that all these variables should have been included under the 'max' signs in (15a) and (16a)). This type of problem is referred to as one of 'simultaneous analysis and design' (SAND), cf. Bendsøe (2006), and is a *very large* problem in the present context. Therefore, we refrain from solving the current topology optimization problems in this form in our paper.

In the form written above, where only the design variables ρ_e, e=1, $\cdots$, N_E, and the bound parameters β and β_1, β_2 is included under the 'max' signs in (15a) and

(16a); the topology optimization problems (15a–c) and (16a–d) are *nondifferentiable* because the eigenfrequencies ω_j, j=1, ⋯, J are considered as functions of the design variables ρ_e, e=1, ⋯, N_E. This is a 'nested' formulation that provides the basis for numerical solution by a scheme of successive iterations where, in each iteration, the eigenfrequencies ω_j and eigenvectors ϕ_j, j=1, ⋯, J are established for known design, ρ_e, e=1, ⋯, N_E, by solution of the generalized eigenvalue problem (7b) and implementation of the orthonormality condition (7c).

To accommodate for possible occurrence of multiple eigenfrequencies, we in the subsequent Section 3.4 consider some important sensitivity results for such eigenfrequencies. In Section 3.5, we make use of these results in the development of incremental forms of problems (15a–c) and (16a–d), which provide the basis for construction of a highly efficient scheme for numerical solution of the topology optimization problems under study.

3.4 Sensitivity analysis of multiple eigenfrequencies

Multiple eigenfrequencies may manifest themselves in different ways in structural optimization problems. One possibility is that an eigenfrequency subject to optimization is multiple from the beginning of the design process, e.g., because of structural symmetries, but an originally unimodal eigenfrequency may also become multiple during the optimization process because of coalescence with one (or more) of its adjacent eigenfrequencies. In this case, sensitivities of the multiple eigenfrequency cannot be calculated straightforwardly from (10) (or (11)) because of the lack of usual differentiability properties of the subspace spanned by the eigenvectors associated with the multiple eigenfrequency. Investigations of sensitivity analysis of multiple eigenvalues (eigenfrequencies or buckling loads) are available in many papers (see, e.g., Bratus and Seyranian 1983a,b; Masur 1984, 1985; Haug et al. 1986; Seyranian 1987a,b; Overton 1988; Seyranian et al. 1994; and papers cited therein).

Following Seyranian et al. (1994), let us assume that the solution of the generalized eigenvalue problem (7b) included in problems (15a–c) or (16a–d) yields a N-fold multiple eigenvalue $\widetilde{\lambda}$,

$$\widetilde{\lambda} = \lambda_j = \omega_j^2, \quad j = n, \cdots, n+N-1 \tag{17}$$

associated with the N (N>1) lowest eigenfrequencies ω_j appearing in the bound constraints (15b) and (16b).[1] In this equation, we shall assume $n+N-1<J$, i.e., that the total number J of eigenfrequencies (counted with multiplicity) considered in problems (15a–c) and (16a–d), is chosen such that the Jth eigenfrequency ω_J is larger than the multiple eigenfrequency corresponding to $\widetilde{\lambda}$ in (17). The multiplicity of the eigenvalue $\widetilde{\lambda}$ in (17) implies that any linear combination of the eigenvectors $\phi_j, j = n, \cdots, n+N-1$, corresponding to $\widetilde{\lambda}$, will satisfy the generalized eigenvalue problem (7b) in (15a–c) and (16a–d), which implies that the eigenvectors are not unique.

In Seyranian et al. (1994), the sensitivity analysis is based on a mathematical perturbation analysis of the multiple eigenvalue and the corresponding eigenvectors. This analysis involves directional derivatives in the design space and leads to the result that the increments $\Delta\lambda_j$ of a multiple eigenvalue $\widetilde{\lambda} = \lambda_j = \omega_j^2, j = n, \cdots, n+N-1$, as in (17) are eigenvalues of a N-dimensional algebraic subeigenvalue problem of the form

$$\det\left[\mathbf{f}_{sk}^{\mathrm{T}}\Delta\rho - \delta_{sk}\Delta\lambda\right] = 0, \quad s,k = n,\ldots,n+N-1, \tag{18}$$

where δ_{sk} is Kronecker's delta, and $\boldsymbol{f}_{\mathrm{sk}}$ denote generalized gradient vectors of the form

$$\mathbf{f}_{sk} = \left\{\phi_s^{\mathrm{T}}\left(\mathbf{K}'_{\rho_1} - \widetilde{\lambda}\mathbf{M}'_{\rho_1}\right)\phi_k, \cdots, \phi_s^{\mathrm{T}}\left(\mathbf{K}'_{\rho_{N_E}} - \widetilde{\lambda}\mathbf{M}'_{\rho_{N_E}}\right)\phi_k\right\}^{\mathrm{T}},$$
$$s,k = n,\ \ldots, n+N-1. \tag{19}$$

According to the definition in (19), each $\boldsymbol{f}_{\mathrm{sk}}$ is a N_E-dimensional vector, and $\mathbf{f}_{sk}^{\mathrm{T}}\Delta\rho$ in (18) is a scalar product for each s, k=n, ..., n+N− 1. The label 'generalized gradient vector' for $\boldsymbol{f}_{sk}$ becomes apparent when comparing (19) with the expression for the gradient vector $\nabla\lambda_j$ of a simple eigenvalue λ_j in (14). Note also that $\boldsymbol{f}_{sk}$=$\boldsymbol{f}_{ks}$ because of the symmetry of the matrices $\mathbf{K}$ and $\mathbf{M}$ and that the two subscripts s and k refer to the orthonormalized eigenmodes from which $\boldsymbol{f}_{sk}$ is calculated.

Assuming that we know the multiple eigenvalue $\widetilde{\lambda}$, the associated subset of orthonormalized eigenmodes, and have computed the derivatives of the matrices $\mathbf{K}$ and $\mathbf{M}$, we can construct the generalized gradient vectors $\boldsymbol{f}_{sk}$, s, k=n, ..., n+N− 1 from (19). Solving the algebraic subeigenvalue problem in (18) for $\Delta\lambda$ then yields the increments $\Delta\lambda = \Delta\lambda_j, j = n, \cdots, n+N-1$, of the multiple eigenvalue $\widetilde{\lambda}$ subject to a given vector $\Delta\rho = \left\{\Delta\rho_1, \cdots, \Delta\rho_{N_E}\right\}$ of increments of the design variables.

The N increments $\Delta\lambda_j, j = n, \cdots, n+N-1$, constitute the eigenvalues of the subeigenvalue problem (18) and represent the directional derivatives of the members of the multiple eigenvalue $\widetilde{\lambda} = \lambda_j = \omega_j^2, j = n, \cdots, n+N-1$, with respect to change $\Delta\rho_e$ of the design variables $\rho_e, e = 1, \cdots, N_E$. Attention should be drawn to the fact that

[1] Similarly, the eigenvalue problem (7b) contained in problem (16a-d) may yield another R-fold eigenvalue $\widehat{\lambda} = \lambda_j = \omega_j^2, j = n-R, \cdots, n-1$, which corresponds to the R largest eigenfrequencies ω_j in (16c). This case (for which we assume that $1 \le n-R$) is completely analogous to (17).

the increments $\Delta\lambda_j, j = n, \cdots, n+N-1$ of the multiple eigenvalue are generally nonlinear functions of the direction of the design increment vector $\Delta\rho$. Thus, unlike simple eigenvalues, multiple eigenvalues do not admit a usual linearization in terms of the design variables.

Finally, two important special cases should be observed.

3.4.1 Case of simple eigenfrequency

As is to be expected, for N=1, i.e., j=s=k=n, (17) and (18) reduce to the case of a simple (unimodal) eigenvalue $\lambda_n = \omega_n^2$. In this case, (18) reduces to the simple algebraic equation

$$\mathbf{f}_{nn}^{\mathrm{T}} \Delta\rho - \Delta\lambda_n = 0, \tag{20}$$

where, according to (13), (19), and (14), we have

$$\mathbf{f}_{nn} = \nabla\lambda_n, \tag{21}$$

i.e., $\mathbf{f}_{nn}$ is simply the vector of sensitivities of the unimodal eigenvalue $\lambda_n = \omega_n^2$ with respect to the design variables ρ_e, e=1, ..., N_E, cf. (10) and (14).

3.4.2 Case of vanishing off-diagonal terms

For the case of multiple eigenvalues, cf. (17) with N>1, a very important observation can be made. If in (18) all off-diagonal scalar products are 0, i.e., if

$$\mathbf{f}_{sk}^{\mathrm{T}} \Delta\rho = 0, \quad s \neq k, \quad s,k = n, \cdots, n+N-1, \tag{22}$$

then the increment $\Delta\lambda_j$ of an eigenvalue $\lambda_j = \omega_j^2$ becomes determined as

$$\Delta\lambda_j = \mathbf{f}_{jj}^{\mathrm{T}} \Delta\rho, \quad j = n, \cdots, n+N-1, \tag{23}$$

where, according to (17) and (19),

$$\mathbf{f}_{jj} = \left\{ \phi_j^{\mathrm{T}} \left(\mathbf{K}'_{\rho_1} - \lambda_j \mathbf{M}'_{\rho_1} \right) \phi_j, \cdots, \phi_j^{\mathrm{T}} \left(\mathbf{K}'_{\rho_{N_E}} - \lambda_j \mathbf{M}'_{\rho_{N_E}} \right) \phi_j \right\}^{\mathrm{T}}, \quad j = n, \cdots, n+N-1. \tag{24}$$

Hence, if the design increment vector $\Delta\rho$ fulfils (22), then $\mathbf{f}_{jj}$ has precisely the same form as the gradient vector $\nabla\lambda_j$ in (14) for a simple eigenvalue, and the eigenvalue increments $\Delta\lambda_j$ in (23) are uniquely determined on the basis of the eigenmodes φ_j, $j = n, \cdots, n+N-1$. The formulas for design sensitivity analysis of multiple eigenvalues then become precisely the same as those for simple eigenvalues.

3.5 Computational procedure

The topology optimization problems (15a–c) and (16a–d) can be efficiently solved by the iterative procedure indicated in Fig. 1, which is applicable for problems with any mix of multiple and simple eigenfrequencies. Firstly, we specify the value of the order n of the eigenfrequency ω_n to be considered, and assign initial values to the design variables ρ_e, $e = 1, \cdots, N_E$. As shown in Fig. 1, the procedure consists of a main (outer) loop and an inner loop, and these shall be briefly discussed in the following.

3.5.1 Main loop

In general, the first step of a given iteration in the main loop is solely based on the given value of n and the set of values of the design variables $\rho_e, e = 1, \cdots, N_E$, obtained at the end of the preceding iteration. Using these values, we first apply (3) to compute the global stiffness and mass matrices $\mathbf{K}$ and $\mathbf{M}$ and then solve the generalized eigenvalue problem (7b) by finite element (FE) analysis for the

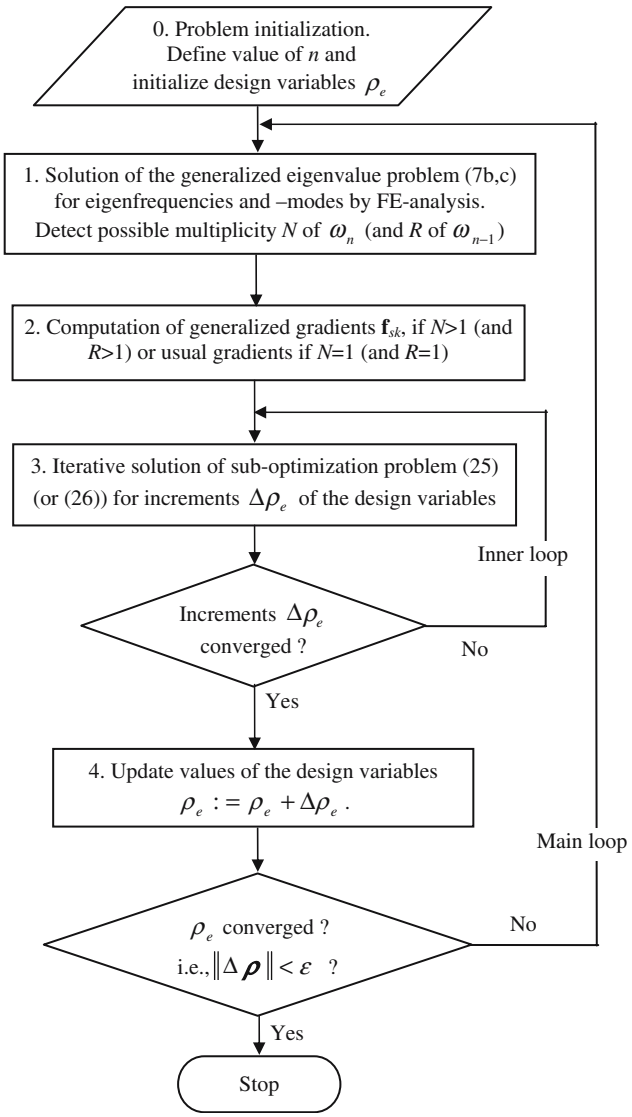

Fig. 1 Flow chart of the iterative solution procedure

eigenfrequencies ω_j and eigenmodes $\phi_j, j = 1, \cdots, J$. In this equation, J must be chosen to be sufficiently large to capture all members of a possible N-fold eigenfrequency $\omega_n = \cdots = \omega_{n+N-1}$. If not done by the FE program, we orthonormalize $\phi_j, j = 1, \cdots, J$ according to (7c).

As an important part of the first step, we finally detect the possible multiplicity N of the eigenfrequency $\omega_n = \cdots = \omega_{n+N-1}$ (as well as multiplicity R of $\omega_{n-R} = \cdots = \omega_{n-1}$ if problem (16a–d) is considered). In this context, the term 'multiplicity' is used if the numerical value of the relative difference between eigenfrequencies in question is within a predefined, very small tolerance.

In the second step of the main loop, we set $\widetilde{\lambda} = \omega_n^2$ (17) (and $\widehat{\lambda} = \omega_{n-1}^2$ for problem (16a–d)), and on the basis of the iterates $\mathbf{K}$, $\mathbf{M}$, ϕ_j, N (and R) obtained in the first step, we now compute $\mathbf{K}'_{\rho_e}$ and $\mathbf{M}'_{\rho_e}$ and subsequently establish the generalized gradient vectors $\mathbf{f}_{sk}, s, k = n, \cdots, n+N-1$, from (19). If problem (16a–d) is considered, $\mathbf{f}_{sk}, s, k = n-R, \cdots, n-1$ also needs to be computed. Note that according to (21), we have $\mathbf{f}_{sk} = \mathbf{f}_{nn} = \nabla(\omega_n^2)$ if ω_n is simple (N=1) and the analogous result if ω_{n-1} is simple (R=1).

In addition to the values of the design variables $\rho_e, e = 1, \cdots, N_E$ used in the first step, all the iterates determined in this and the second step, i.e., $\mathbf{K}$, $\mathbf{M}$, ω_j, and $\phi_j, (j = 1, \cdots, J)$, N, R, $\widetilde{\lambda}$, $\widehat{\lambda}$, and the $\mathbf{f}_{sk}$ vectors mentioned above are kept fixed in the third step of the main loop.

As indicated in Fig. 1, the third step of the main loop consists of an inner loop that solves a suboptimization problem. Upon convergence, this inner loop delivers optimum values of increments $\Delta\rho_e, e = 1, \cdots, N_E$ of the design variables subject to the fixed values of the above mentioned iterates. The inner loop is discussed below.

In the fourth step of the main loop, the design variables ρ_e, $e = 1, \cdots, N_E$, are updated by addition of the increments $\Delta\rho_e$, and subsequently, a check for convergence of ρ_e is performed by investigating whether the norm of the vector $\Delta\rho = (\Delta\rho_1, \cdots, \Delta\rho_{N_E})$ of design increments is less than a small, predefined value ε. If the design variables ρ_e have converged, the optimum topology design has been obtained—otherwise, the updated vector of design variables is used as a basis for a subsequent iteration in the main loop.

3.5.2 Inner loop

Inspired by the results (18) and (19) of the sensitivity analysis of a multiple eigenfrequency in Section 3.4, we shall now develop a scheme to be used in the third step of the main loop in Fig. 1 for optimum values of increments $\Delta\rho_e, e = 1, \cdots, N_E$ of the design variables subject to the known values of iterates that are fixed in the third step. To this end, we rewrite the bound formulations (15a–c) and (16a–d) in terms of the vector $\Delta\rho$ of increments $\Delta\rho_e$, $e = 1, \cdots, N_E$, of the design variables and corresponding increments of the squared eigenfrequencies $\Delta\lambda_j = \Delta(\omega_j^2), j = n, \cdots, n+N-1$ (and $j = n-R, \cdots, n-1$, for problem (16a–d)). Hereby, we obtain the following subproblems to be solved for optimum increments in the third step of the main loop of the computational procedure for:

(1) Maximization of the nth eigenfrequency:

$$\max_{\beta, \Delta\rho_1, \cdots, \Delta\rho_{N_E}} \{\beta\} \tag{25a}$$

subject to:

$$\beta - \left[\omega_j^2 + \mathbf{f}_{jj}^{\mathrm{T}} \Delta\rho\right] \le 0, \quad \text{for j} = \text{J} = \text{n} + \text{N}, \tag{25b}$$

$$\beta - \left[\omega_j^2 + \Delta(\omega_j^2)\right] \le 0, \quad j = n, \ldots, n+N-1, \tag{25c}$$

$$\det\left[\mathbf{f}_{sk}^T \Delta\rho - \delta_{sk}(\omega^2)\right] = 0, \quad s, k = n, \ldots, n+N-1, \tag{25d}$$

$$\sum_{e=1}^{N_E} (\rho_e + \Delta\rho_e) V_e - V* \le 0, \quad V* = \alpha V_0, \tag{25e}$$

$$0 < \underline{\rho} \le \rho_e + \Delta\rho_e \le 1, \quad e = 1, \cdots, N_E, \tag{25f}$$

(2) Maximization of the gap (distance) between the nth and $(n-1)$st eigenfrequencies:

$$\max_{\beta_1, \beta_2, \Delta\rho_1, \cdots \Delta\rho_{N_E}} \{\beta_2 - \beta_1\} \tag{26a}$$

subject to:

$$\beta_2 - \left[\omega_j^2 + \mathbf{f}_{jj}^{\mathrm{T}} \Delta\rho\right] \le 0, \quad \text{for } j = J = n+N, \tag{26b}$$

$$\beta_2 - \left[\omega_j^2 + \Delta(\omega_j^2)\right] \le 0, \quad j = n, \ldots, n+N-1, \tag{26c}$$

$$\left[\omega_j^2 + \Delta(\omega_j^2)\right] - \beta_1 \le 0, \quad j = n-R, \ldots, n-1, \quad (R \le n-1) \tag{26d}$$

$$\left[\omega_j^2 + \mathbf{f}_{jj}^{\mathrm{T}} \Delta\rho\right] - \beta_1 \le 0, \quad \text{for } j = n-R-1, \quad (\text{if } R \le n-2) \tag{26e}$$

$$\det\left[f_{sk}^{\mathrm{T}}\Delta\rho - \delta_{sk}(\omega^2)\right] = 0, \quad s,k = n,\ldots,n+N-1, \tag{26f}$$

$$\det\left[\mathbf{f}_{sk}^{\mathrm{T}}\Delta\rho - \delta_{sk}(\omega^2)\right] = 0, \quad s,k = n-R,\ldots,n-1, \tag{26g}$$

$$\sum_{e=1}^{N_E}(\rho_e + \Delta\rho_e)V_e - V^* \le 0, \quad V^* = \alpha V_0, \tag{26h}$$

$$0 < \underline{\rho} \le \rho_e + \Delta\rho_e \le 1, \quad e = 1,\cdots,N_E. \tag{26i}$$

Note that we have not transferred to (25a–f) and (26a–i), respectively, the constraints in (15a–c) and (16a–d) containing the generalized eigenvalue problem (7b) and orthonormality conditions (7c); these constraints have been already implemented through the structural FE analysis in step 1 of the main loop of the iterative solution procedure, cf. Section 3.5.1 and Fig. 1. Note also that in the suboptimization problems (25a–f) and (26a–i), the only unknowns are the bound variables β and (β_1, β_2) and the increments of the design variables $\Delta\rho_e$, $e = 1, \cdots, N_E$, which play the role as independent variables, and the dependent variables are the increments $\Delta(\omega_j^2), j = n, \cdots, n+N-1$ of the N-fold eigenfrequency $\omega_n^2 = \cdots = \omega_{n+N-1}^2$ (in problems (25a–f) and (26a–i)) together with the increments $\Delta\left(\omega_j^2\right), j = n-R, \cdots, n-1$ of the R-fold eigenfrequency $\omega_{n-R}^2 = \cdots = \omega_{n-1}^2$ (in problem (26a–i)). All other iterates in (25a–f) and (26a–i), i.e., the material volume densities ρ_e, the eigenfrequencies ω_j, the generalized gradient vectors $\mathbf{f}_{sk}$, and the multiplicities N and R have been determined in steps 1 and 2 of the main iteration loop and are kept fixed in the current step 3 of this loop.

Earlier, we defined J as the highest order of an eigenfrequency to be considered and subjected to the variable bound constraints (15b) and (16b) in problems (15a–c) and (16a–d). In the current computational procedure, we have chosen J to be the order J=n+N of the closest eigenfrequency that is greater than the multiple eigenfrequency $\omega_j, j = n+N-1$. Assuming that the Jth eigenfrequency is simple, it immediately follows from Section 3.4.1 that the variable bound constraint for the incremented form of the Jth eigenfrequency can be written as (25b) and (26b) in problems (25a–f) and (26a–i). A corresponding constraint for the closest eigenfrequency ω_{n-R-1} that is smaller than the multiple eigenfrequency $\omega_j^2, j = n-R, \cdots, n-1$ takes the form (26e), if ω_{n-R-1} is simple.

3.5.3 Remarks

It is seen that relative to (15a–c) and (16a–d), (25d), (26f), and (26g) have been included in the formulations of problems (25a–f) and (26a–i). These equations stem from (18) and represent the coupling between the independent variables $\Delta\rho_e$ and the dependent variables $\Delta\left(\omega_j^2\right)$ corresponding to multiple eigenfrequencies. This coupling is nonlinear in general. Each of (25d), (26f), and (26g) represent an algebraic subeigenvalue problem with $\Delta(\omega^2)$ as an eigenvalue that furnishes a number of solutions $\Delta\left(\omega_j^2\right)$, which correspond to the possible multiplicity N of the eigenvalue (17) in problems (15a–c) and (16a–d) and the possible multiplicity R of the additional similar eigenvalue that may occur in problem (16a–d) and is defined in the earlier footnote. The increments $\Delta(\omega_j^2)$ obtained this way are seen to enter the variable bound constraints (25c), (26c), and (26d) for the incremented multiple eigenfrequencies. Note that if N and/or R have been found to be equal to unity in step 1 of the main (outer) loop in Fig. 1, it follows directly from the results in Section 3.4.1 that each of (25d), (26f), and/or (26g) reduce to the pertinent single algebraic equation for the increment of a simple eigenfrequency.

This means that the computational procedure developed in the present Section 3.5 and outlined in Fig. 1, can be applied for automatic solution of problems (15a–c) and (16a–d) in Section 3.3 independently of whether the subject eigenfrequencies of order n in (15a–c) and (16a–d) and of order $n-1$ in (16a–d) are members of a multiple eigenvalue or are just a simple eigenvalue.

The suboptimization problems (25a–f) and (26a–i) of problems (15a–c) and (16a–d), respectively, can be solved by using a mathematical programming method. In this paper, the MMA method (Svanberg 1987) has been used.

Finally, it is worth noting that if we introduce the additional constraints $\mathbf{f}_{sk}^{\mathrm{T}}\Delta\rho = 0$, for $s \neq k$, s, k=n, ..., n+N−1, i.e., if we impose vanishing of the off-diagonal terms in (18), then the increments $\Delta\lambda_j = \Delta(\omega_j^2)$ are determined in a linearized form with respect to the increments $\Delta\rho_e$ of the material volume densities for both simple and multiple eigenvalues. As a result, the suboptimization problems (25a–f) and (26a–i) reduce to linear programming problems (see Krog and Olhoff 1999) and can be solved using a linear programming algorithm.

4 Numerical examples: single material topology design of beam-like 2D structures

4.1 Maximization of the fundamental eigenfrequency

As a first example, we consider the topology optimization of a single-material beam-like structure modeled by 2D

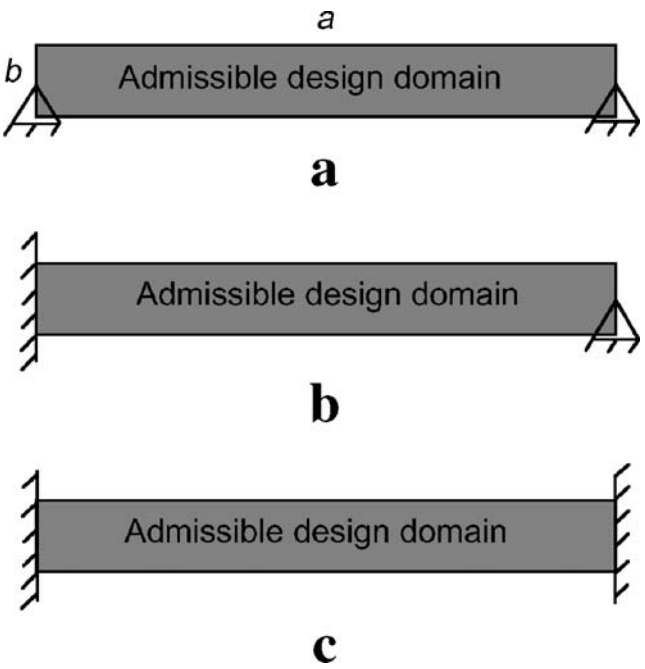

Fig. 2 **a**–**c** Admissible design domains (a=8, b=1) of beam-like 2D structures with three different sets of boundary conditions. **a** Simply supported ends. **b** One end clamped, the other simply supported. **c** Clamped ends. The fundamental eigenfrequencies of the three initial designs (uniform distribution of material with density ρ=0.5) are all unimodal with values $\omega_{1a}^{\phi} = 68.7$, $\omega_{1b}^{\phi} = 104.1$, and $\omega_{1c}^{0} = 146.1$

plane stress elements. The admissible design domain is specified, and three different cases a, b, and c of boundary conditions as shown in Fig. 2 and defined in the caption are considered. The design objective is to maximize the fundamental eigenfrequency for a prescribed material volume fraction α=50%, and in the initial design, the available material is uniformly distributed over the admis-

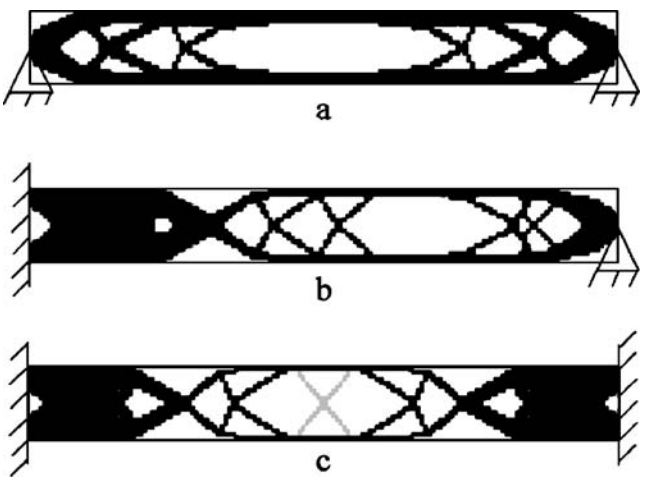

Fig. 3 **a**–**c** Optimized single-material topologies (50% volume fraction) for the three different sets of boundary conditions defined in Fig. 2a–c. The optimum fundamental eigenfrequencies are all found to be bimodal and have the values **a** $\omega_{1a}^{opt} = 174.7$, **b** $\omega_{1b}^{opt} = 288.7$, and **c** $\omega_{1c}^{opt} = 456.4$, implying that they are increased by **a** 154, **b** 177, and **c** 212% relative to the initial designs

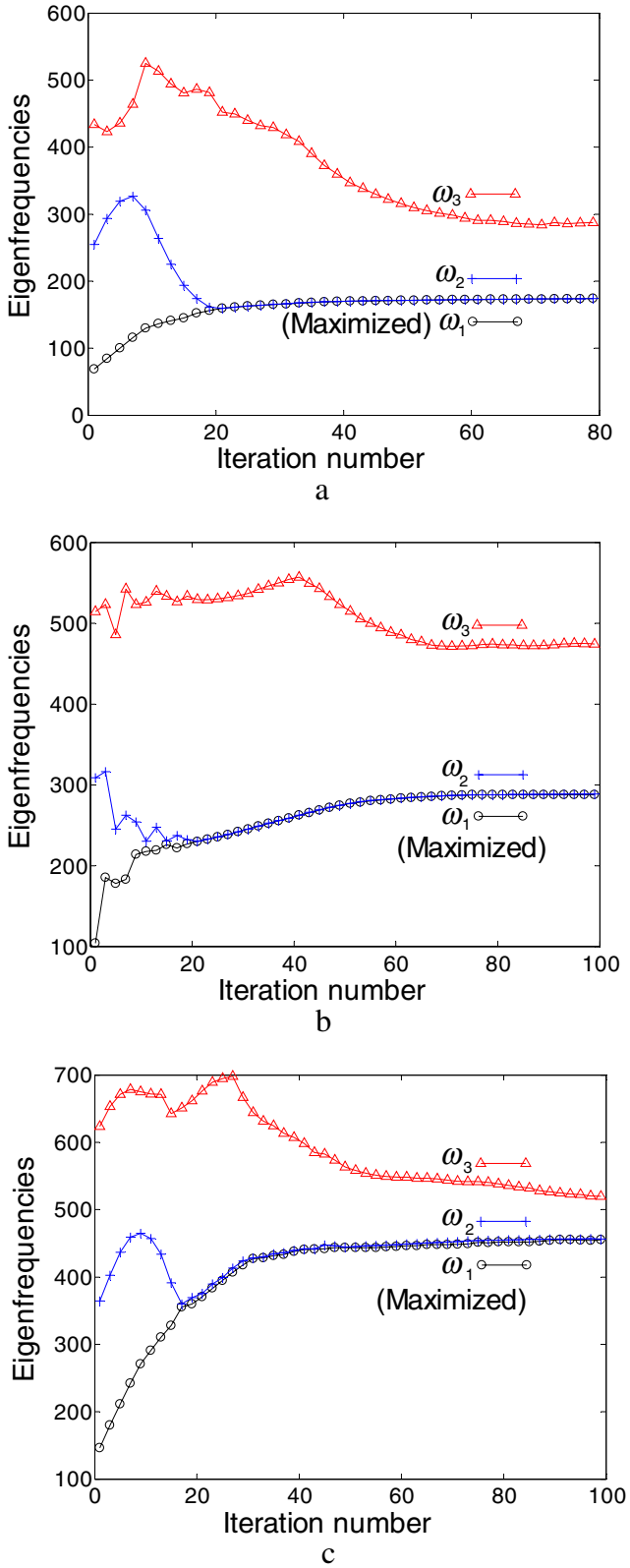

Fig. 4 **a**–**c** Iteration histories of the first three eigenfrequencies associated with the design process leading to the results in Fig. 3a–c. It is seen that for each of the three cases, the fundamental eigenfrequency is simple for the initial design but soon coalesces with the second eigenfrequency. Thus, the maximized fundamental eigenfrequencies for all three cases are bimodal

sible design domain. The material is isotropic with Young's modulus $E=10^7$, Poisson's ratio $\upsilon=0.3$, and mass density $\rho_m=1$ (SI units are used throughout). The fundamental eigenfrequencies of the initial designs with the three cases (a), (b) and (c) of boundary conditions are given in the caption of Fig. 2. The optimized topologies are shown in Fig. 3a–c, and the corresponding optimum fundamental eigenfrequencies are all bimodal with values given in the caption of Fig. 3. Iteration histories of the first three eigenfrequencies for each of the three cases of boundary conditions are given in Fig. 4. Figure 5a–c depicts the first three eigenmodes of the optimized 2D structure with simply supported ends as shown in Fig. 3a. The results indicate that the first two eigenmodes (corresponding to the bimodal fundamental eigenfrequency) of the structure are typical simply supported beam-type vibration modes, and the third one is a more general 2D vibration mode.

4.2 A comparison of the present approach with early attempts of topology optimization with respect to eigenfrequencies

In early attempts to extend the original static compliance topology design methodology pioneered by Bendsøe and Kikuchi (1988) and Bendsøe (1989) to eigenvalue optimization problems, the authors (see, e.g., Diaz and Kikuchi 1992; Ma et al. 1994, 1995; Diaz et al. 1994; Kosaka and Swan 1999) developed different design objective functions defined as weighted sums or other combinations of eigenfrequencies. These objective functions were constructed with a view to avoid switching of orders of subject eigenfrequencies during the optimization process because of multiple eigenfrequencies, which gave rise to severe discontinuities in the sensitivity of the objective function and lack of convergence of the computations.

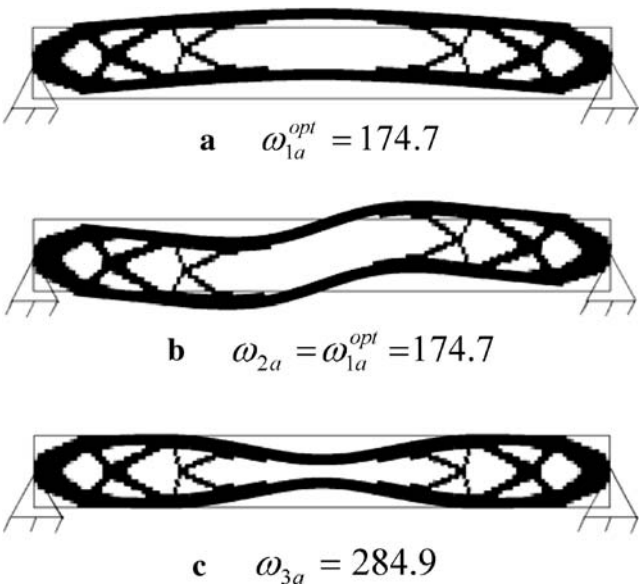

Fig. 5 a–c The three first eigenmodes of the simply supported structure in Fig. 3a with a bimodal optimum fundamental eigenfrequency. **a** and **b** depict the two modes associated with the optimum fundamental eigenfrequency, and **c** shows the subsequent mode

Fig. 6 Single-material topology design (50% volume fraction) obtained by maximizing the first eigenfrequency of the simply supported beam-like structure in Fig. 2a by the using the mean eigenvalue approach. The design may be compared with the optimum design in Fig. 3a

In this section, we briefly present an example for comparison of the method developed in the present paper and a method based on a specially developed objective function of the type mentioned above. For a fair comparison, we choose one of the best of these methods, namely, the so-called mean-eigenvalue approach (see Ma et al. 1995), where the design objective is defined as a mean eigenvalue λ^*, which is a combination of several consecutive eigenfrequencies of the structure. A typical form of such a mean eigenvalue is

$$\lambda^* = \left(\sum_{j=n}^{n+L-1} \frac{1}{\omega_j^2} \right)^{-1}, \tag{27}$$

where ω_j ($j=n$, $n+1$, ..., $n+L-1$) are the eigenfrequencies considered. From (27), it is seen that the lowest eigenfrequency (i.e., ω_n) plays the dominant role in the objective function λ^*, and maximization of λ^* will normally yield the

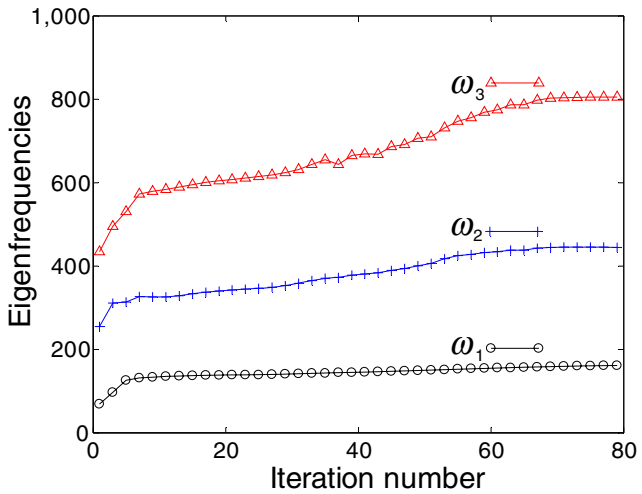

Fig. 7 Iteration history of the first three eigenfrequencies associated with the design process leading to the topology design in Fig. 6. Note that that the variations of the second and third eigenfrequencies are quite different from those in Fig. 4a for the optimum design

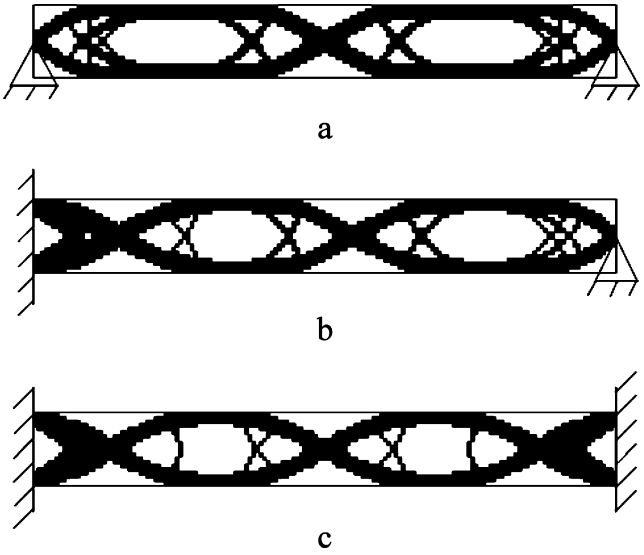

Fig. 8 **a**–**c** Optimized single-material topologies (50% volume fraction) for the three different sets of boundary conditions in Fig. 2a–c. The optimum second eigenfrequencies are found to be **a** $\omega_{2a}^{opt} = 598.3$, **b** $\omega_{2b}^{opt} = 732.8$, and **c** $\omega_{2c}^{opt} = 849.0$, and are all bimodal

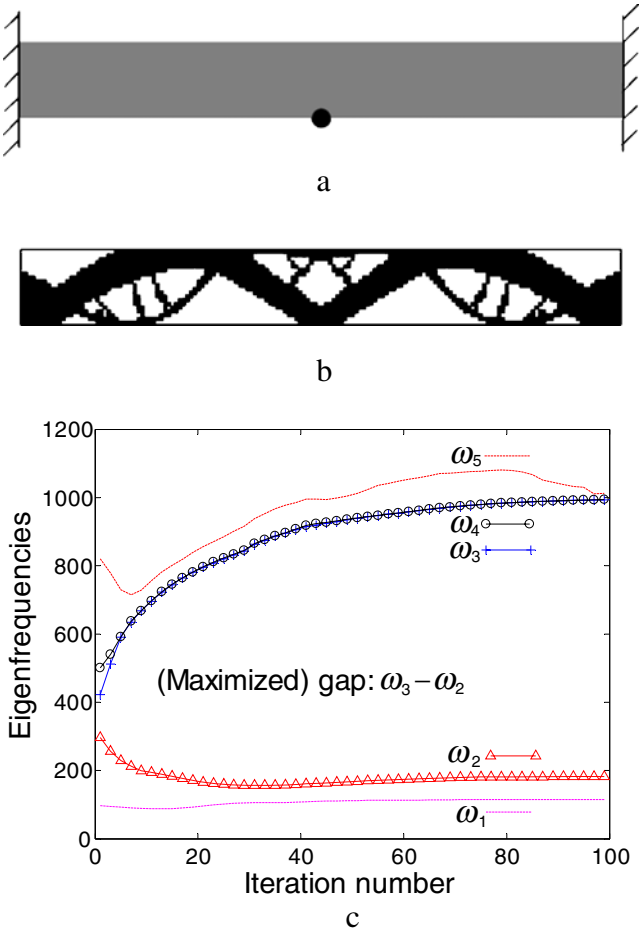

Fig. 9 **a** A clamped beam-like 2D structure with a concentrated mass attached at the midpoint of the lower edge. **b** Optimized topology of the beam-like structure. The gap between the second and the third eigenfrequencies is maximized. **c** Iteration histories for the first five eigenfrequencies associated with the process leading to the design (**b**)

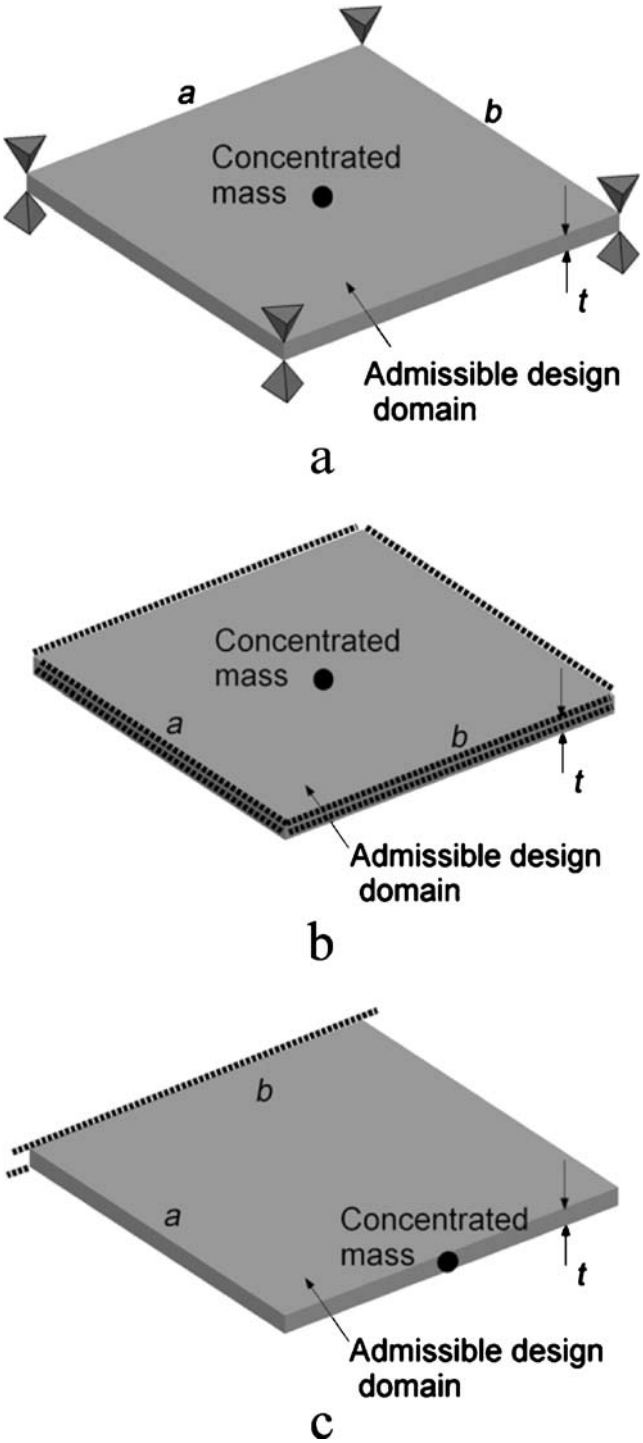

Fig. 10 Quadratic plate-like 3D structure (a=20, b=20, and t=1) with three different cases of boundary conditions and attachment of a concentrated nonstructural mass. **a** Simple supports at four corners and concentrated mass m_c at the center of the structure ($m_c = m_0/3$, m_0 the total structural mass of the plate). **b** Four edges clamped and concentrated mass m_c at the center ($m_c = m_0/10$). **c** One edge clamped, other edges free, and concentrated mass m_c attached at the mid-point of the edge opposite to the clamped one ($m_c = m_0/10$). The fundamental eigenfrequencies for the three initial designs (uniform distribution of material with density ρ=0.5) are $\omega_{1a}^0 = 8.1$, $\omega_{1b}^0 = 31.1$, and $\omega_{1c}^0 = 3.5$

largest relative increase in the lowest eigenfrequency ω_n in comparison with the other eigenfrequencies considered. Thus, maximization of the objective function (27) can be used to obtain an approximation to the optimum value of the nth eigenfrequency ω_n.

Figure 6 shows the result of applying the mean eigenvalue approach to "optimizing" the topology of the simply supported beam-like structure (with the initial design in Fig. 2a), with respect to its fundamental eigenfrequency. The design objective λ^* is defined as the combination of the first three eigenfrequencies in (27); that is, we have set n=1 and L=3 in (27). We see that that the design is different from the optimum design in Fig. 3a obtained by the method presented in the present paper, in the sense that some thin beam or truss components appear in the middle part of the structure.

As a result, we find that the first eigenfrequency of the structure in Fig. 6 is simple and has the value $\omega_1 = 161.7$, which is *lower* than the (bimodal) first eigenfrequency $\omega_{1a}^{opt} = 174.7$ of the optimum structure in Fig. 3a, which *confirms the superiority of the approach presented in the present paper.*

Figure 7 shows the iteration history of the first three eigenfrequencies of the structure in Fig. 6 obtained by the mean eigenvalue approach. Relative to the iteration history of the corresponding eigenfrequencies in Fig. 4a of the optimum solution in Fig. 3a, it is seen that a coalescence of the first and second eigenfrequencies does not occur by using the mean eigenvalue approach because of quite large increases of the second (and also the third) eigenfrequency during the computational procedure (see Fig. 7). Actually, the second and third eigenfrequencies of the structure in Fig. 6 are found to be $\omega_2 = 444.5$ and $\omega_3 = 805.6$, respectively, which are substantially larger than the corresponding eigenfrequencies $\omega_{2a} = \omega_{1a}^{opt} = 174.7$ and $\omega_{3a} = 284.9$ of the optimum design in Fig. 3a, cf. the captions of Fig. 5b,c.

Examples of maximizing higher order eigenfrequencies by usage of the mean eigenvalue approach have also been carried out. These also confirmed the superiority of the method presented in this paper.

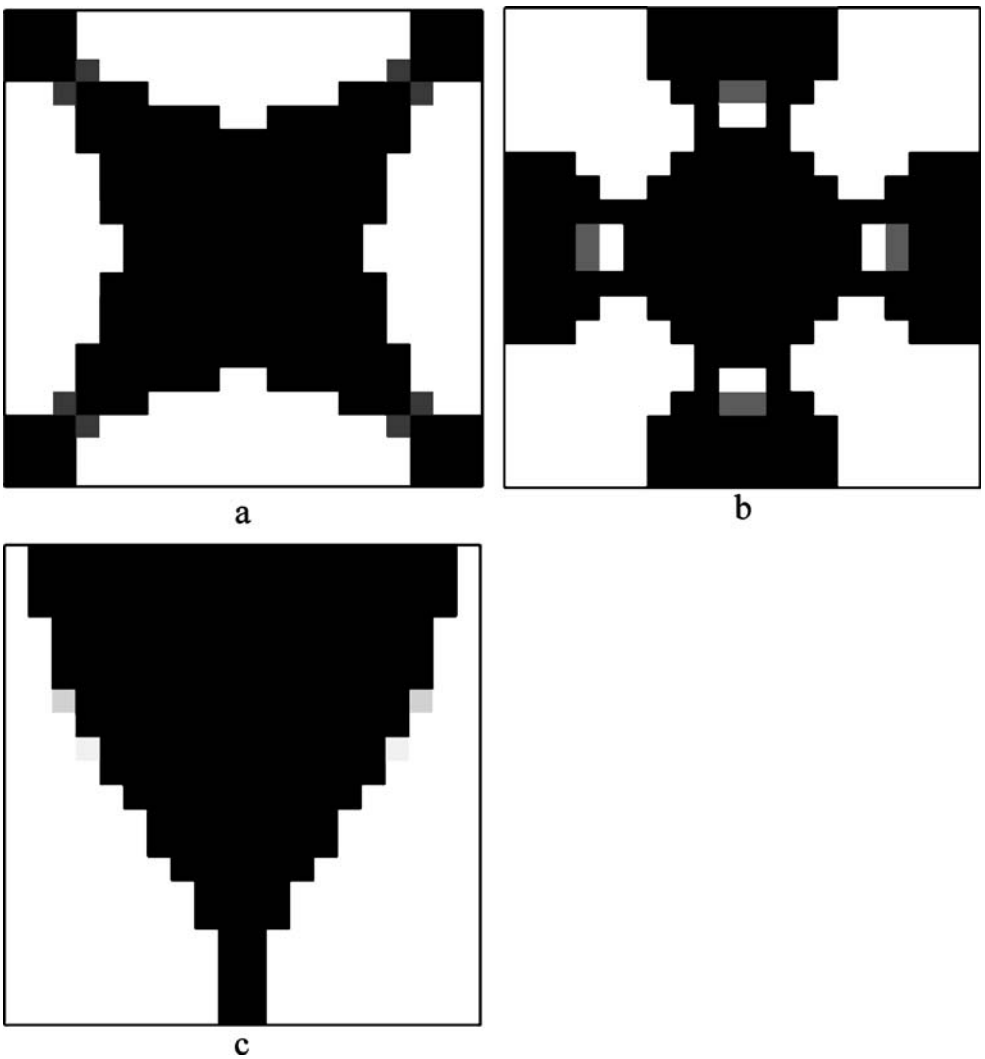

Fig. 11 **a**–**c** Optimized single-material topologies (50% volume fraction) for the three different cases of boundary conditions and mass attachment in Fig. 10a–c. The optimum fundamental eigenfrequencies are found to be **a** $\omega_{1a}^{opt} = 16.4$, **b** $\omega_{1b}^{opt} = 65.4$, and **c** $\omega_{1c}^{opt} = 9.7$, implying that they are increased by **a** 101, **b** 111, and **c** 179% relative to the initial designs

4.3 Maximization of the second eigenfrequency

In the remainder of the paper, we return to applications of the formulations and methodology developed in the present paper and now present an example of topology optimization of single material beam-like structures for maximum value of the second eigenfrequency. The initial data and the three sets of boundary conditions in this example are the same as for the first example in Section 4.1. The resulting topologies are shown in Fig. 8a–c.

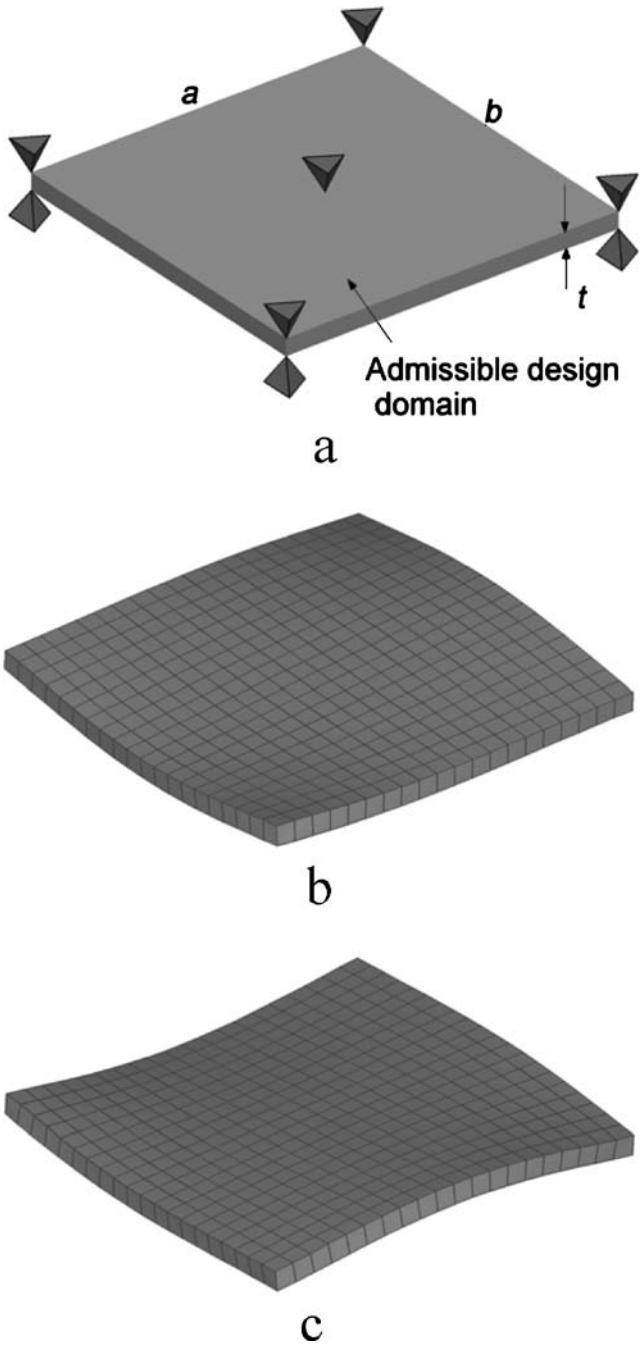

Fig. 12 Quadratic plate-like 3D structure (a=20, b=20, and t=1) with simple supports at its four corners and center. **a** Admissible design domain. **b**–**c** The eigenmodes of the initial design associated with the bimodal fundamental eigenfrequency $\omega_1^0 = \omega_2^0 = 24.6$

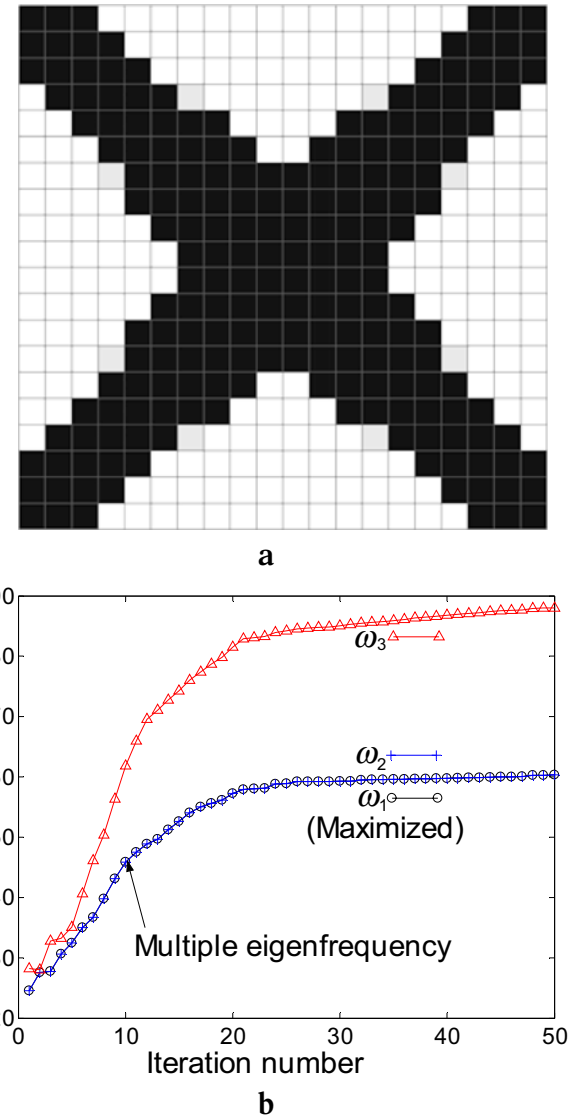

Fig. 13 **a** Optimized topology (50% volume fraction, single-material design) associated with the maximum fundamental eigenfrequency $\omega_1^{opt} = 60.3$, which is bimodal. **b** Iteration history for the first three eigenfrequencies

4.4 Maximization of the distance (gap) between two consecutive eigenfrequencies

In this example, we consider the design objective of maximizing the distance (gap) between two consecutive

Fig. 14 **a**–**c** Optimized single-material topologies (50% volume fraction) corresponding to the three different cases of boundary conditions and mass attachment in Fig. 10a–c. The values and multiplicities of the optimum second eigenfrequencies are **a** $\omega_{2a}^{opt} = 46.0$ (trimodal), **b** $\omega_{2b}^{opt} = 155.4$ (bimodal), and **c** $\omega_{2c}^{opt} = 39.8$ (bimodal) ▶

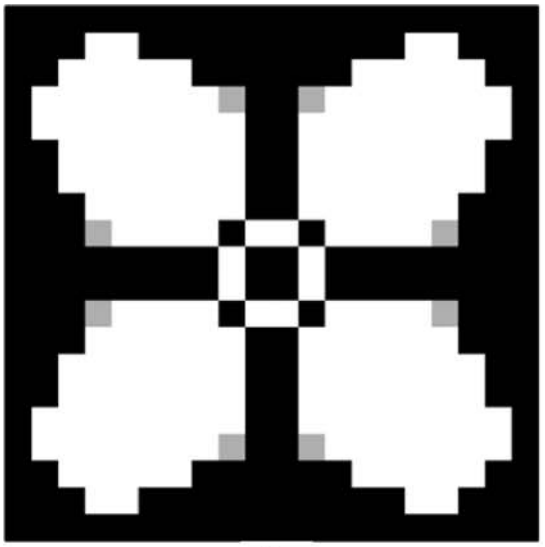

a

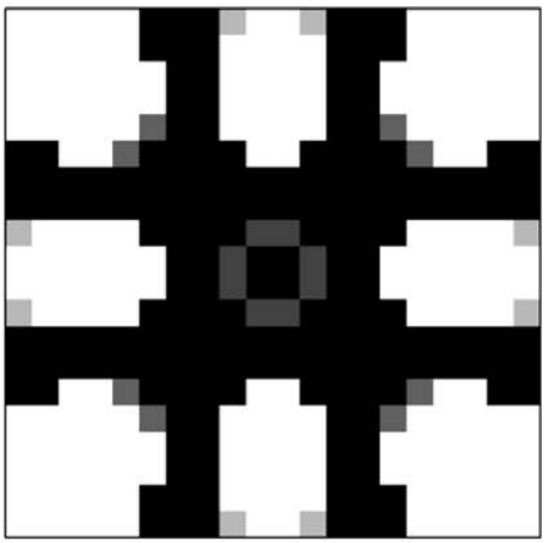

b

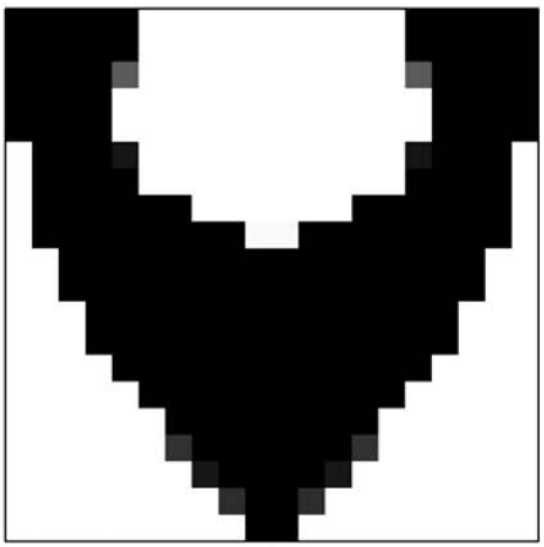

c

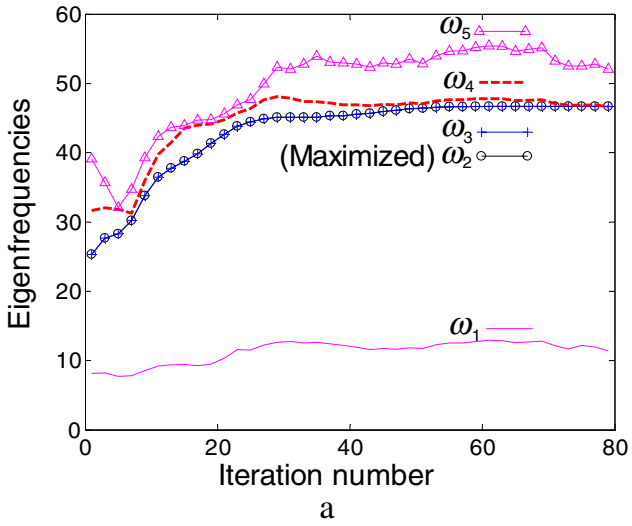

a

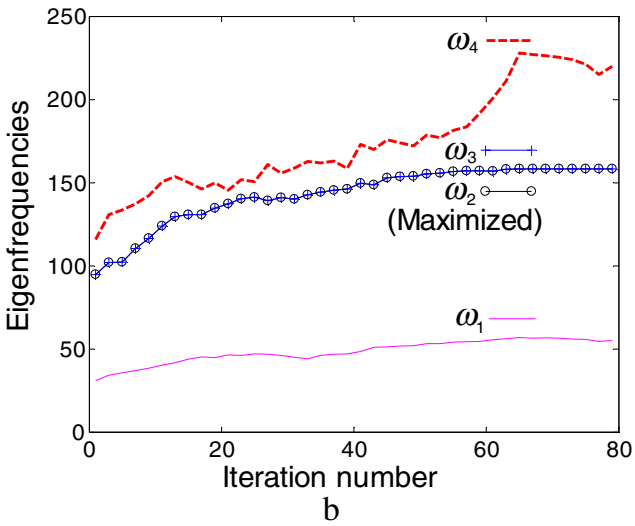

b

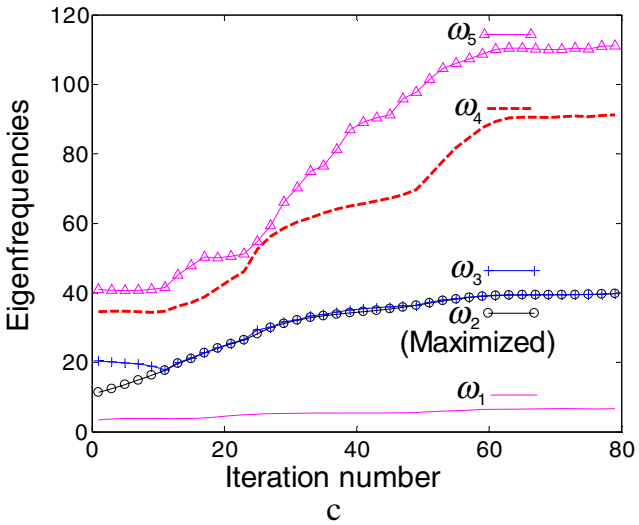

c

Fig. 15 Iteration histories of eigenfrequencies associated with the design process leading to the results in Fig. 14a–c. For case **c**, it is seen that the second eigenfrequency is simple for the initial design but soon coalesces with the third eigenfrequency

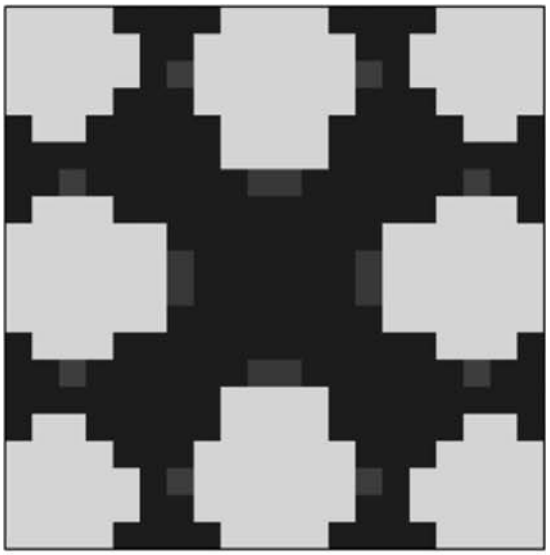

a

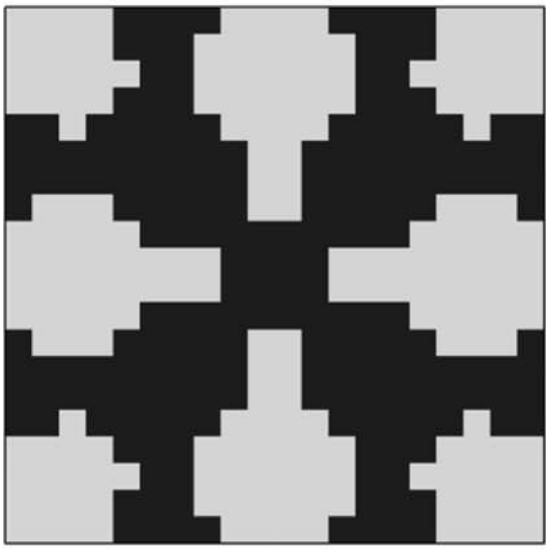

b

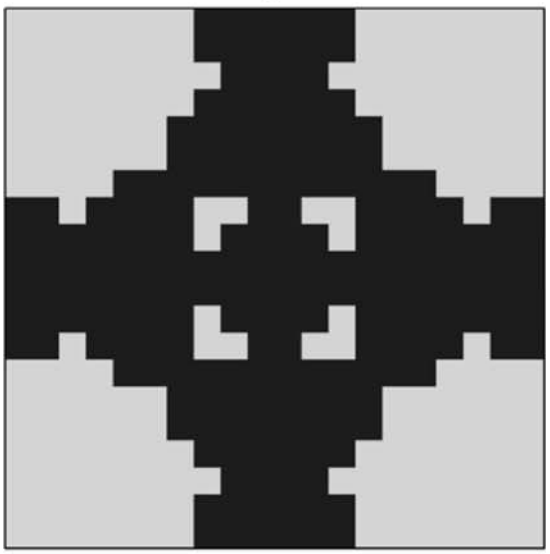

c

◀ **Fig. 16** Optimized topologies of the bimaterial plate with all edges clamped and a concentrated mass attached to the center, cf. Fig. 10b. The topologies correspond to maximum values of the **a** fourth, **b** fifth, and **c** sixth eigenfrequency. The stiffer and the weaker materials are indicated by *black* and *gray*, respectively, and the volume fraction of the stiffer material *1 is 50%

eigenfrequencies (the second and the third eigenfrequencies) of the clamped beam-like structure shown in Fig. 9a. A concentrated, nonstructural mass m_c is attached at the midpoint of the lower edge of the design domain as shown in Fig. 9a. The attached mass has the value $m_c = 1/2 m_b$, where m_b denotes the given mass of total structural material for the beam. We use the same admissible design domain, boundary conditions, structural material, and volume fraction as in the example shown in Fig. 2c.

The optimum topology and the corresponding iteration histories of the eigenfrequencies of the present example are depicted in Fig. 9b and c. It is seen that the second eigenfrequency is decreased, whereas the third eigenfrequency is increased. We find that the design ends up with a maximized gap between the second and the third eigenfrequencies that is equal to 810, which is no less than 548% larger than the difference between the corresponding eigenfrequencies of the initial design. Figure 9c shows that already from the first few iterations, the third and fourth eigenfrequencies form a bimodal eigenfrequency, which, at the end of the iteration history, coalesces with the fifth eigenfrequency and thereby becomes a trimodal eigenfrequency in the final optimum design.

5 Numerical examples: topology design of plate-like 3D structures

In this section, we present examples of topology optimization of both single and bimaterial plate-like structures. The structures are modeled by eight-node 3D continuum finite elements with Wilson-incompatible displacement models to improve precision.

5.1 Maximization of the fundamental eigenfrequency of single-material structures

In this section, we consider topology optimization of single-material, initially quadratic plate-like structures with the same admissible design domain, but three different cases a, b, and c of boundary conditions and attached concentrated, nonstructural masses as shown in Fig. 10 and defined in the caption of this figure. The design objective is to maximize the fundamental eigenfrequency for a prescribed material volume fraction $\alpha = 50\%$, and in the initial design, the available material is uniformly distributed over

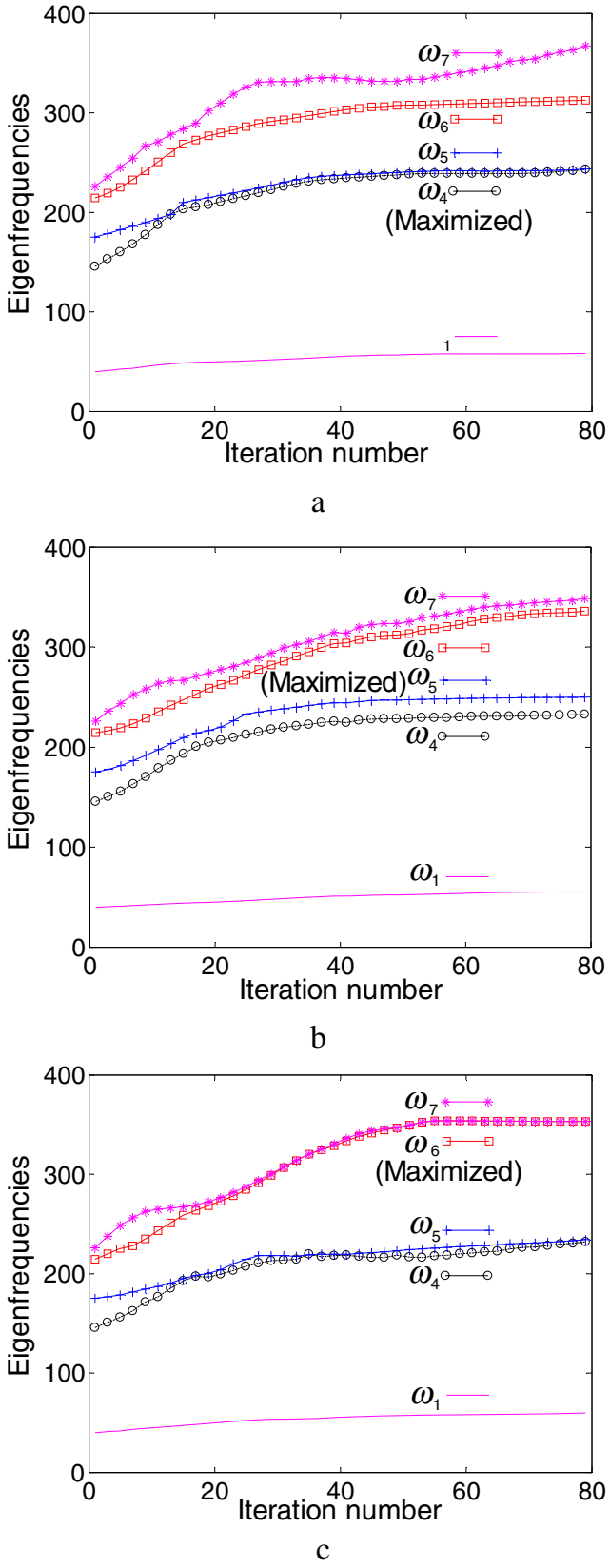

◀ **Fig. 17** Iteration histories of eigenfrequencies associated with the design process leading to the results in Fig. 16a–c. The maximized fourth, fifth, and sixth eigenfrequencies are **a** $\omega_{4b}^{\mathrm{opt}} = 243.8$ (bimodal), **b** $\omega_{5b}^{\mathrm{opt}} = 249.7$ (unimodal), and **c** $\omega_{6b}^{\mathrm{opt}} = 353.2$ (bimodal). The graphs for $\omega?\omega_2$ and $\omega?\omega_3$ are omitted in figures in order to make these less crowded

the admissible design domain. The material is isotropic with Young's modulus $E=10^{11}$, Poisson's ratio $\upsilon=0.3$, and mass density $\rho_{\mathrm{m}}=7{,}800$ (SI units are used throughout). The fundamental eigenfrequencies of the initial designs with the three cases a, b, and c of boundary/mass conditions are

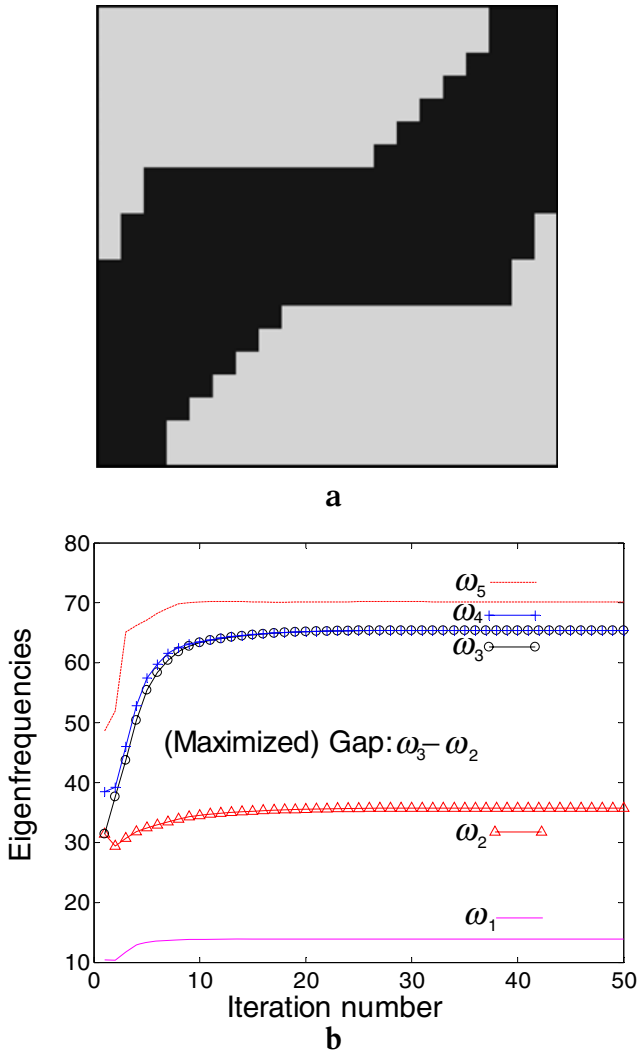

Fig. 18 **a** Optimized topology of a bimaterial, quadratic plate-like structure with simple supports at four corners and a concentrated mass at the center, cf. Fig. 10a. The design objective is to maximize the distance between the second and the third eigenfrequencies. **b** Iteration histories for the first five eigenfrequencies associated with the optimization process leading to the design (**a**). Note that the second and third eigenfrequencies of the initial design form a double (bimodal) eigenfrequency but that they split very early in the design process and have a large distance in the optimum design. It is also seen in **b** that the initially distinct third and fourth eigenfrequencies very early coalesce and form a bimodal eigenfrequency of the optimum design

given in the caption of Fig. 10. The optimized plate topologies are shown in Fig. 11a–c, and the corresponding optimum fundamental eigenfrequencies are all unimodal with values given in the caption of Fig. 11.

As a next example, single-material topology optimization of an initially quadratic plate-like structure with simple supports at its four corners and center is considered (Fig. 12a). The admissible design domain and the material are the same as in the foregoing example. Because of the structural symmetry, the fundamental eigenfrequency of the initial design is bimodal with modes shown in Fig. 12b–c. The optimized topology is shown in Fig. 13a (50% volume fraction). The corresponding optimum fundamental eigenfrequency is also bimodal.

5.2 Maximization of higher order eigenfrequencies for single- and bimaterial structures

In this section, we first present an example of topology optimization of initially quadratic single-material structures with respect to the second eigenfrequency. The initial data for the example are the same as for the first example in Section 5.1. Thus, we choose the same volume and type of available material, the same admissible design domain, and again consider the three different cases a, b, and c of boundary conditions and attached concentrated masses as shown in Fig. 10, but we now maximize the second eigenfrequencies. The resulting optimum topologies and the frequency iteration histories for the three cases of boundary conditions and mass attachment in Fig. 10 are given in Figs. 14 and 15.

In the next example, we consider topology optimization of bimaterial structures with respect to higher order eigenfrequencies. Both of the two materials are isotropic. The stiffer material *1 with elasticity and mass matrices $\mathbf{E}_e^{*1}, \mathbf{M}_e^{*1}$, see Section 2.3, is indicated by black in Fig. 16 and is the same as that used for optimization with a single-material in the preceding examples. The weaker material *2 is indicated by gray in Fig. 16 and has the properties $\mathbf{E}_e^{*2} = 0.1\mathbf{E}_e^{*1}$ and $\mathbf{M}_e^{*2} = 0.1\mathbf{M}_e^{*1}$. We take the volume fraction of material *1 to be 50% and present results of optimizing the topologies of a bimaterial quadratic plate with the same boundary conditions and attachment of a concentrated mass as shown in Fig. 10b. Figure 16a–c shows the optimized plate topologies associated with maximum values of the fourth, fifth, and sixth eigenfrequencies, and Fig. 17a–c shows the corresponding iteration histories of the eigenfrequencies.

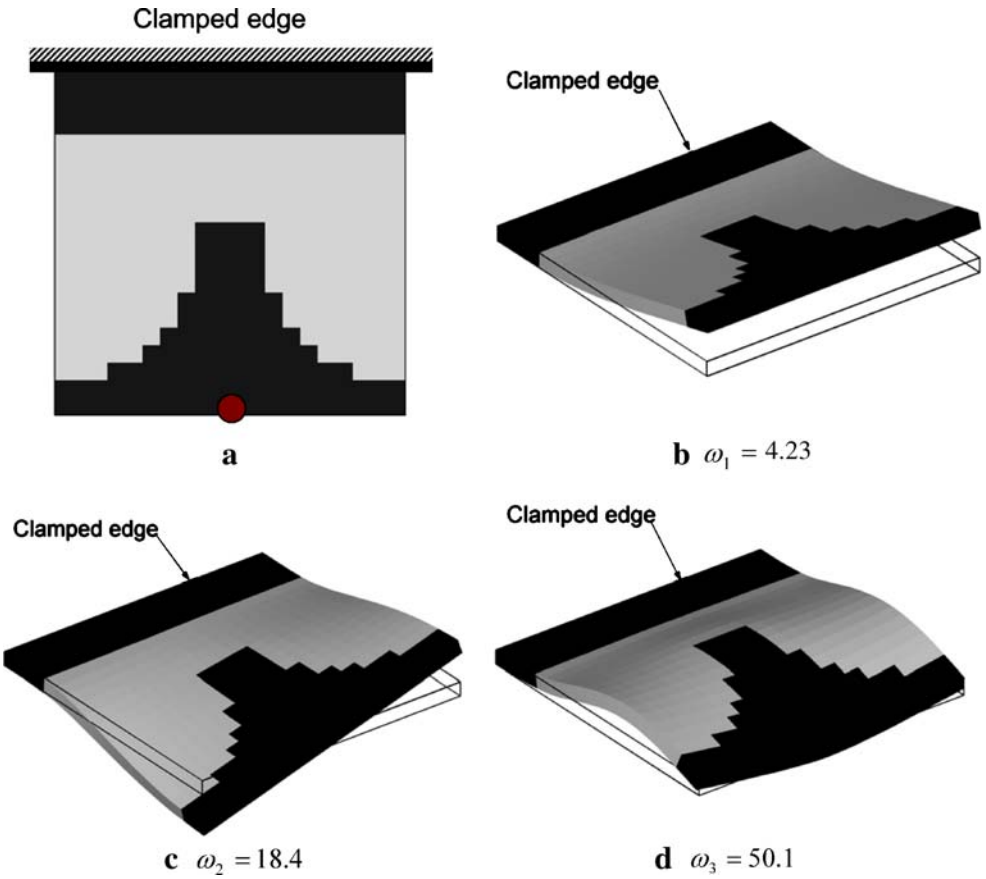

Fig. 19 **a** Optimized topology of the plate-like structure defined in Fig. 10c with the upper horizontal edge clamped, other edges free, and a concentrated mass attached at the midpoint of the lower horizontal edge. **b–d** The first, second, and third eigenmodes of the optimized bimaterial plate topology. The gap between the second and the third eigenfrequencies is maximized, $(\omega_3 - \omega_2)_{\text{opt}} = 31.7$

5.3 Maximization of the distance (gap) between two consecutive eigenfrequencies of bimaterial structures

In this section, we present two examples of topology optimization of bimaterial plate structures, using the same materials and volume fractions as in the previous example. The design objective considered is to maximize the distance (gap) between the second and third eigenfrequencies of the structures. We use the same admissible quadratic design domain as in Fig. 10 for the plate structures and choose the cases a and c of boundary conditions and concentrated mass attachment as shown in Fig. 10. The results of the two examples are given in Figs. 18 and 19, respectively.

The result shown in Fig. 18 of the topology optimization of the quadratic, bimaterial plate structure in Fig. 10a with an initially uniform distribution of a homogeneous mixing of equal amounts of the two materials is particularly interesting. Because of the symmetries of the initial design, see Fig. 10a, the difference between the third and second eigenfrequencies is 0 for the initial design. However, the optimum topology of the plate depicted in Fig. 18a has a large gap between its third and second eigenfrequencies, cf. Fig 18b, which implies that the *relative increase* in the difference between these eigenfrequencies is *infinitely large* relative to the initial design!

6 Summary

Problems of topology optimization with respect to eigenfrequencies of free vibrations of structures are presented in this paper. The design objectives are maximization of specific eigenfrequencies and distances (gaps) between two consecutive eigenfrequencies of the structures. A method has been developed to handle topology optimization problems associated with multiple eigenfrequencies and has been implemented in such a way that it can be applied independently of whether the subject eigenfrequencies are multiple or just simple (unimodal). Several numerical examples of topology optimization of single- and bimaterial 2D and plate-like 3D structures are carried out and presented in the paper, where they validate the approaches proposed. The results demonstrate that the creation of structures with multiple optimum eigenfrequencies is the rule rather than the exception in topology optimization of vibrating structures and that this feature needs careful attention. The results also witness that the techniques enable us, in a cost-efficient manner, to move structural resonance frequencies far away from external excitation frequencies and thereby avoid high vibration and noise levels. We show in two sequential papers that the same desirable effects can be achieved by topological design for minimum dynamic compliance (Olhoff and Du 2007) and for minimum sound radiation (Du and Olhoff 2007), respectively, of continuum structures subjected to given excitation frequencies of forced vibration.

Acknowledgments Financial support provided by the Center of Machine Acoustics and Aalborg University is gratefully acknowledged.

References

Bendsøe MP (1989) Optimal shape design as a material distribution problem. Struct Optim 1:193–202

Bendsøe MP (2006) Computational challenges for multi-physics topology optimization. In: Mota Soares CA, Martins JAC, Rodrigues HC, Ambrosio JAC (eds) Computational mechanics—solids, structures and coupled problems. Springer, Dordrecht, The Netherlands, pp 1–20

Bendsøe MP, Kikuchi N (1988) Generating optimal topologies in structural design using a homogenization method. Comput Methods Appl Mech Eng 71(2):197–224

Bendsøe MP, Olhoff N (1985) A method of design against vibration resonance of beams and shafts. Optim Control Appl Methods 6:191–200

Bendsøe MP, Sigmund O (1999) Material interpolation schemes in topology optimization. Arch Appl Mech 69:635–654

Bendsøe MP, Sigmund O (2003) Topology optimization: theory, methods and applications. Springer, Berlin

Bendsøe MP, Olhoff N, Taylor JE (1983) A variational formulation for multicriteria structural optimization. J Struct Mech 11:523–544

Bendsøe MP, Olhoff N, Sigmund O (eds) (2006) Topological design optimization of structures, machines and materials—status and perspectives. Proc. IUTAM Symp., Copenhagen, Denmark, October 26–29, 2005. Springer, Dordrecht, The Netherlands

Bratus AS, Seyranian AP (1983a) Bimodal solutions in eigenvalue optimization problems. Prikl Mat Meh 47:546–554

Bratus AS, Seyranian AP (1983b) Bimodal solutions in eigenvalue optimization problems. Appl Math Mech 47:451–457

Cheng G, Olhoff N (1982) Regularized formulation for optimal design of axisymmetric plates. Int J Solids Struct 18:153–169

Diaz AR, Kikuchi N (1992) Solutions to shape and topology eigenvalue optimization problems using a homogenization method. Int J Numer Methods Eng 35:1487–1502

Diaz AR, Lipton R, Soto CA (1994) A new formulation of the problem of optimum reinforcement of Reissner–Midlin plates. Comp Meth Appl Mechs Eng 123:121–139

Du J, Olhoff N (2007) Minimization of sound radiation from vibrating bi-material structures using topology optimization. Struct Multidiscipl Optim 33:305–321

Eschenauer H, Olhoff N (2001) Topology optimization of continuum structures: a review. Appl Mech Rev 54(4):331–389

Haftka RT, Gurdal Z, Kamat MP (1990) Elements of structural optimization. Kluwer, Dordrecht

Haug EJ, Choi KK, Komkov V (1986) Design sensitivity analysis of structural systems. Academic, New York

Jensen JS, Pedersen NL (2006) On maximal eigenfrequency separation in two-material structures: the 1D and 2D scalar cases. J Sound Vib 289:967–986

Kosaka I, Swan CC (1999) A symmetry reduction method for continuum structural topology optimization. Comput Struct 70:47–61

Krog LA, Olhoff N (1999) Optimum topology and reinforcement design of disk and plate structures with multiple stiffness and eigenfrequency objectives. Comput Struct 72:535–563

Lancaster P (1964) On eigenvalues of matrices dependent on a parameter. Numer Math 6:377–387

Ma ZD, Cheng HC, Kikuchi N (1994) Structural design for obtaining desired eigenfrequencies by using the topology and shape optimization method. Comput Syst Eng 5(1):77–89

Ma ZD, Kikuchi N, Cheng HC (1995) Topological design for vibrating structures. Comput Methods Appl Mech Eng 121:259–280

Masur EF (1984) Optimal structural design under multiple eigenvalue constraints. Int J Solids Struct 20:211–231

Masur EF (1985) Some additional comments on optimal structural design under multiple eigenvalue constraints. Int J Solids Struct 21:117–120

Olhoff N (1976) Optimization of vibrating beams with respect to higher order natural frequencies. J Struct Mech 4:87–122

Olhoff N (1977) Maximizing higher order eigenfrequencies of beams with constraints on the design geometry. J Struct Mech 5:107–134

Olhoff N (1989) Multicriterion structural optimization via bound formulation and mathematical programming. Struct Optim 1:11–17

Olhoff N, Du J (2007) Topological design for minimum dynamic compliance of continuum structures subjected to forced vibration. Struct Multidisc Optim (in press)

Olhoff N, Parbery R (1984) Designing vibrating beams and rotating shafts for maximum difference between adjacent natural frequencies. Int J Solids Struct 20:63–75

Overton ML (1988) On minimizing the maximum eigenvalue of a symmetric matrix. SIAM J Matrix Anal Appl 9(2):256–268

Pedersen NL (2000) Maximization of eigenvalues using topology optimization. Struct Multidisc Optim 20:2–11

Rozvany G, Zhou M (1991) Applications of the COC method in layout optimization. In: Eschenauer H, Mattheck C, Olhoff N (eds) Proc. Int. Conf. on Engineering Optimization in Design Processes (held in Karlsruhe 1990). Springer, Berlin Heidelberg New York, pp 59–70

Rozvany G, Zhou M, Birker T (1992) Generalized shape optimization without homogenization. Struct Optim 4:250–252

Seyranian AP (1987a) Multiple eigenvalues in optimization problems. Prikl Mat Meh 51:349–352

Seyranian AP (1987b) Multiple eigenvalues in optimization problems. Appl Math Mech 51:272–275

Seyranian AP, Lund E, Olhoff N (1994) Multiple eigenvalues in structural optimization problems. Struct Optim 8(4):207–227

Sigmund O (1997) On the design of compliant mechanisms using topology optimization. Mech Struct Mach 25:493–524

Sigmund O (2001) Microstructural design of elastic band gap structures. In: Cheng GD et al (eds), Proceedings of the 4th World Congress of Structrual and Multidisciplinary Optimization WCSMO4. Liaoning Electronic, Dalian, China, pp 6

Sigmund O, Jensen JS (2003) Systematic design of phononic band-gap materials and structures by topology optimization. Philos Trans R Soc Lond Ser A Math Phys Sci 361:1001–1019

Sigmund O, Petersson J (1998) Numerical instabilities in topology optimization: a survey of procedures dealing with checkerboards, mesh-dependencies and local minima. Struct Optim 16:68–75

Svanberg K (1987) The method of moving asymptotes − a new method for structural optimization. Int J Numer Methods Eng 24:359–373

Taylor JE, Bendsøe MP (1984) An interpretation of min–max structural design problems including a method for relaxing constraints. Int J Solids Struct 20:301–314

Tcherniak D (2002) Topology optimization of resonating structures using SIMP method. Int J Numer Methods Eng 54:1605–1622

Wittrick WH (1962) Rates of change of eigenvalues, with reference to buckling and vibration problems. J R Aeronaut Soc 66:590–591